

## Chapter 4

# Biological influences on seafloor carbonate precipitation

Kristin D. Bergmann<sup>1</sup>, John P. Grotzinger<sup>1</sup>, Woodward W. Fischer<sup>1</sup>

<sup>1</sup>California Institute of Technology

*originally published in PALAIOS v. 28 no. 2 p. 99-115 © 2013 SEPM (Society for Sedimentary Geology)*

### 4.1 Abstract

The sedimentary record reveals first-order changes in the locus of carbonate precipitation through time, documented in the decreasing abundance of carbonate precipitation on the seafloor. This pattern is most clearly recorded by the occurrence of seafloor carbonate crystal fans (bladed aragonite pseudomorphs neomorphosed to calcite or dolomite), which have a distinct temporal distribution—ubiquitous in Archean carbonate platforms, but decline through Proterozoic time and are extremely rare in Phanerozoic basins. To understand better the potential influences on this pattern, we built a mathematical framework detailing the effects of organic matter delivery and microbial respiratory metabolisms on the carbonate chemistry of shallow sediments. Two non-unique end-member solutions emerge in

which seafloor precipitation is favorable: enhanced anaerobic respiration of organic matter, and low organic matter delivery to the sediment-water interface. This analysis suggests that not all crystal fans reflect a unique set of circumstances, rather there may have been several different geobiological and sedimentary mechanisms that led to their deposition. We then applied this logical framework to better understand the petrogenesis of two distinct crystal fan occurrences—the late Paleoproterozoic Beechey Formation, Northwest Territories, Canada and the middle Ediacaran Rainstorm Member of the Johnnie Formation, Basin and Range, USA—using a combination of high-resolution petrography, micro x-ray fluorescence and wavelength dispersive spectroscopy, C isotopes, and sedimentary context to invert for geobiological processes occurring at the sediment-water interface. Interestingly, both of these Proterozoic examples are associated with iron-rich secondary mineral assemblages, have elevated trace metal signatures, and sit within maximum flooding intervals, highlighting key commonalities in syn-sedimentary geobiological processes that led to seafloor carbonate precipitation.

## 4.2 Introduction

The sedimentary record demonstrates that large-scale aspects of carbonate deposition have remained unchanged over  $> 3.4$  Ga of Earth history [1]. This reflects long-term commonalities in the sources and sinks of dissolved inorganic carbon (DIC) and alkalinity in seawater and the processes that generate and fill accommodation in sedimentary basins. Despite this stability, the record also reveals important first-order changes, at smaller length scales, in the nature of carbonate precipitation through time, this is documented in the decreasing abundance of seafloor carbonate precipitation (Table 4.1, references therein). Changes in carbonate precipitation dynamics are also evidenced in Precambrian precipitated stromatolite morphologies, herringbone calcite, molar tooth structure and giant ooids [2, 3, 4, 5, 1]. The reemergence of seafloor-precipitated crystal fans in subtidal carbonate environments after Paleoproterozoic time is important because each

example coincides with known carbon cycle perturbations [6, 7, 8]. Uncovering the basis for these occurrences holds an important key to understanding secular changes in the linkages between acid-base and redox processes on the surface Earth [6, 1, 9].

Herein, we explore the potential importance of sediment-water interface chemistry and the impact of microbial respiration on the temporal distribution of seafloor crystal fans through time. We begin with methods and results from a mathematical model exploring the effects of organic matter delivery and different respiratory metabolisms on the carbonate chemistry of the sediment-water interface. This framework makes specific predictions for the signature of biologically influenced precipitation that we then test with a variety of sedimentologic, petrographic, and isotopic observations. We focused on two Proterozoic crystal fan-containing deposits widely distributed in time—the late Paleoproterozoic Beechey Formation, Northwest Territories, Canada and the middle Ediacaran Rainstorm Member of the Johnnie Formation, Basin and Range, USA. We show observations from a range of high-resolution petrographic techniques that provide insight into the sedimentary geochemistry of the environments in which they grew.

#### **4.2.1 Occurrences of aragonite seafloor crystal fans in the sedimentary record**

Subtidal aragonite seafloor-precipitated crystal fans were first described from the Paleoproterozoic Odjick-Rocknest transition, Canada [10]. Since then, many occurrences of seafloor aragonite pseudomorphs have been documented in carbonate successions. These occurrences were compiled in Grotzinger (1989) and in Grotzinger and James (2000). An updated tabulation is shown in Table 4.1. A crucial outcome of the existing body of work is the distinct temporal distribution of carbonate crystal fans. They are ubiquitous in Archean carbonate platforms, common in late Paleoproterozoic carbonate platforms and are restricted to peritidal environments during Mesoproterozoic time [2, 1]. There are noticeable gaps in the crystal fan record between 3.5 Ga and 3 Ga, between 2.5 Ga and 2 Ga,

and between  $\sim 580$  Ma and the present, except for Permian and Early Triassic occurrences (Table 4.1). During Precambrian time, wherein the record of preserved carbonates is scarcer and the age constraints are fewer, the temporal distribution likely reflects both a true change in carbonate depositional style as well as a strong bias associated with the preserved rock record. In general, the record gets poorer with age, and yet even with a diminished record, crystal fans are an important component of the few preserved Archean carbonate platforms (e.g., [11, 12]). Here the signal clearly stands out from the bias. That in mind, the scarcity of carbonate platforms of middle Archean and early Paleoproterozoic age highlights the likelihood that both the 3.5 Ga to 3 Ga gap and 2.5 Ga and 2 Ga gap may be directly due to record bias. As summarized previously [2, 1], subtidal crystal fans reminiscent of Archean and late Paleoproterozoic seafloor crystal fans reappear in Neoproterozoic and Phanerozoic successions during periods of perturbation to the ocean-atmosphere system—most notably directly overlying the cap carbonate dolostones associated with the Marinoan glaciation [13, 14, 15, 16, 17, 18, 19, 20] and around the Permian-Triassic mass extinction [6, 21, 22, 23, 24]. The sedimentary record of the past 630 million years is, in many ways, much clearer and far more continuous, yet during this interval seafloor-precipitated fabrics are not ever a common component of carbonate platforms.

The striking nature of this long-term temporal pattern has generated a variety of explanations [4, 1, 9]. Broadly, the distribution of  $\text{CaCO}_3$  precipitation and dissolution within the ocean is dependent on the size of the DIC reservoir, the pressure and temperature dependent solubility of carbonate minerals, and the strength and metabolisms of organic carbon production and respiration. In modern ocean basins, large gradients in carbonate saturation state between surface and deep seawater exists because of a strong biological pump, high  $\text{pO}_2$  and aerobic respiration of organic carbon [9, 25]. A longstanding interpretation of the temporal distribution of crystal fan occurrences has involved a decrease in surface seawater carbonate saturation state through time [26, 4, 1]. Under this hypothesis, Archean oceans were characterized by highly supersaturated surface seawater and crystal

Best Age (Ma)	Location & Reference	Context
3,450	Strelley Pool Formation, Waarrawoona Greenstone Belt, Western Australia (Grotzinger, 1989; Allwood et al., 2009)	Flat pebble conglomerates assoc. with crystal fans
2,940	Uchi Greenstone Belt, Canada (Sumner and Grotzinger, 2000)	
2,700	Cheshire Formation, Belingwe Greenstone Belt, Zimbabwe (Grotzinger, 1989; Sumner and Grotzinger, 2000; Hofmann, et al., 2004), Steep Rock Group, Canada (Grotzinger, 1989; Kusky and Hudleston, 1999; Sumner and Grotzinger, 2000)	Cheshire Fm. -- Crystal fans grow from erosional surfaces and lag deposits of detrital sediments, intimately associated with microbial laminae. Steep Rock Group -- within fenestral microbial laminae
2,600	Huntsman Formation, Zimbabwe (Sumner and Grotzinger, 2000; Hofmann, et al., 2004), Carawine Formation, Australia (Sumner and Grotzinger, 2000)	Huntsman Fm. -- Crystal fans are interbedded with interpreted microbial laminae and black coatings. Carawine Fm. -- draped in sediments and sometimes reworked
2,540	Campbellrand-Malmani Platform, South Africa (Sumner and Grotzinger, 2000; Sumner and Grotzinger, 2004)	Found in subtidal through supratidal depositional environments
2,500	Yellowknife Supergroup, Canada (Grotzinger, 1989)	
1,970	Beechey Formation, Canada (Grotzinger and Friedman, 1989; Grotzinger, 1993)	Crystal fans associated with granular iron formation, sit on transgressive surface
1,900	Odjick-Rocknest Boundary, Canada (Grotzinger and Reed, 1983),	Thin authigenic hematite coatings on crystal fans, sit on transgressive surface
1,880	Pethei Group, Canada (Sami and James, 1996)	
1,640	Teena Formation, McArthur Group, Australia (Winefield, 2000)	Crystal fans interbedded with pink carbonates and sit at the transgressive surface
1,400	Gaoyuzhuang Formation, China (Seong-Joo and Golubic, 2000), Kotuikan Formation, Siberia (Bartley, et al., 2000)	Gaoyuzhuang Fm. -- Crystal fans associated with "sediment rich layers" and are red-brown in color. Both crystal fan occurrences are peritidal.
1,200	Ruyang Group, China (Xiao et al., 1997)	Crystal fans draped by darker, micritic laminae, blades highlighted by organic matter or hematite
1,100	Society Cliffs Formation, Canada (Kah and Knoll, 1996)	Peritidal crystal fans associated with evaporites
740	Bambui Group, Brazil (Peryt, et al., 1990; Babinski et al., 2007)	High Sr concentrations, Crystal fans are grey in color and are associated with red lime mudstones
667?	Pocatello Formation, United States (Corsetti et al., 2004; Lorentz et al., 2004)	Crystal fans are associated with pink limestones and are draped with micritic or siliclastic sediments.
630	Maieberg Formation, Namibia (Hoffman et al., 1998; Hoffman, et al., 2007), Mt. Doreen Formation, Australia (Kennedy, 1996), Bushmansklippe Formation, Namibia (Saylor, et al., 1998), Hayhook Formation, Canada (James, et al., 2001), Mirasol d'Oeste Formation, Brazil (Font, et al., 2006), Ol Member, Tsagaan Oloom Formation (Macdonald, et al., 2009), Katakuruk Formation, Alaska (Clough and Goldammer, 2000; Macdonald, et al., 2009)	Crystal fans sit at the dolomite-limestone transition associated with the maximum flooding interval following the Marinoan Glaciation. They are often associated with pink limestones, authigenic minerals and microbial laminae. Detrital hematite is noted in the Maieberg Formation.
580	Johnnie Formation, United States (Summa, 1993; Pruss, et al., 2008)	Sit at the maximum flooding interval, dense detrital grains particularly hematite are associated with the crystal fans and nucleation surface
265	Capitan Reef, United States (Grotzinger and Knoll, 1995)	Reef cavity botryoids, no known examples of direct precipitation on the seafloor
252	Shareza Formation, Iran (Baud, et al., 2007), Abedah, Turkey (Heydari and Hassanzadeh, 2003; Heydari, et al., 2003), Kokarkuyu Formation, Turkey (Pruss, et al., 2006), Guizhou, China (Payne, et al., 2007), Cekic Dagı Formation, Turkey (Payne, et al., 2007), Mitai and Kamura Formations, Japan (Payne, et al., 2007),	In the Shareza and Kokarkuyu Fms. the crystal fans are forming on flooded or drowning platforms.
251	Alwa Formation, Oman (Woods and Baud, 2008)	Iron-manganese coatings described within sequence that contains crystal fans

Table 4.1: Ages, geological names, references and significant context of documented crystal fans occurrences from the sedimentary record.

fans would have formed during rapid precipitation events. Higgins et al. (2009) proposed that periods of abundant in situ seafloor precipitation were characterized by a small gradient in carbonate saturation from the surface to the deep ocean, controlled by widespread anaerobic respiration of organic carbon and a large DIC reservoir and/or a weak biological pump. In this framework, the temporal decline of seafloor-precipitated textures preserved in Precambrian carbonate platforms can be explained as a product of increasing  $pO_2$  and aerobic respiration of organic carbon as well as decreasing  $pCO_2$  and a shrinking DIC reservoir [27, 9].

One key to understanding the nature of seafloor carbonate fans is recognition that these features were influenced by and record mass fluxes across the sediment-water interface. Despite strongly supersaturated seawater with respect to both aragonite and calcite over modern carbonate platforms, this style of seafloor precipitation does not occur today. Today, dissolution in shallow sediments near the sediment-water interface is driven by the aerobic respiration of organic matter (and oxidation of other sedimentary reductants like sulfide), which increases aqueous  $CO_2$ , consumes alkalinity, and lowers pH [28, 29, 30, 31]. This highlights the importance of local gradients in carbonate saturation state, these gradients are due in large part to the effects of biology, and have changed over the course of Earth history.

### **4.3 Carbonate chemistry at the sediment-water interface**

Supersaturated surface waters overlying modern carbonate platforms should drive carbonate seafloor precipitation based on thermodynamic predictions ( $\Omega > 1$ ), and many studies have shown that supersaturated seawater does indeed result in the inorganic precipitation of carbonate minerals. The location of these precipitates in the modern ocean, however, is telling [32, 33, 34, 35, 36]. Aragonite precipitates have been documented within reef cavities as large botryoidal fans and as fine needles precipitated on carbonate grains suspended in the water column at 30

and 60 m depth [33, 35]. Inorganic precipitation also occurs from seawater onto pre-existing aragonite needles during whittings events [32, 36, 37]. Other types of carbonate precipitates exist within modern carbonate supersaturated environments but these sit more clearly within a continuum of biologically mediated and abiotic precipitates, these include ooids and various cements including hardground, beachrock, and stromatolite cements [38, 39, 40, 41].

If tropical surface seawater ( $\Omega_{\text{aragonite}} \sim 3$ ) can produce aragonite precipitates, the question of why these features do not form on the seafloor in the modern becomes an important juxtaposition against the occurrences of seafloor precipitates in the rock record. Seawater is not uniform with regard to its carbonate chemistry, and processes occurring in shallow sediments and at the sediment-water interface play an important role in the probability of crystal fan nucleation and growth. The dominant controls on whether precipitation is viable at the sediment-water interface include the acid-base and redox chemistry occurring on the seafloor and in shallow sediments, the balance between the kinetics of carbonate precipitation rate and background sedimentation rate, and physical processes like bioturbation that drive mixing and perturb mass flux across the sediment-water interface.

Studies of carbonate platform environments reveal evidence for carbonate dissolution in near-surface sediments through a complex set of processes [28, 29, 42, 30, 31]. Both aerobic respiration and sulfate reduction decrease the pH in sediment pore waters undergoing organic diagenesis [43, 28]. On carbonate platforms, pore water profiles indicate sulfate reduction begins within 5 cm of the sediment-water interface in many environments [28, 30]. Furthermore, with limited iron concentrations in shallow carbonate environments, the hydrogen sulfide produced during sulfate reduction diffuses upward and is reoxidized (commonly by  $\text{O}_2$ ) in shallower sediments or at the sediment-water interface, often associated with bioturbation [29, 42]. The oxidation of the hydrogen sulfide produces the bulk of the acidity contributing to the dissolution of carbonate phases with smaller contributions from aerobic respiration and sulfate reduction [29]. The accumulation of  $\text{Ca}^{2+}$  and  $\text{CO}_3^{2-}$  ions in the pore fluids driven by microbial respiration and

carbonate dissolution can result in carbonate precipitation (and cementation) at greater depths in the sediments but not commonly near the sediment-water interface [30]. Thus, the combined effect of the two dominant microbial respiration pathways (in modern ocean basins) and the two-fold effects of bioturbation—both physical disruption of the sediment-water interface and promoting hydrogen sulfide oxidation—serve as important chemical and physical hindrances to seafloor-precipitated crystal fans on modern carbonate platforms. Ultimately these studies reveal that geobiological processes that include the synthesis and respiration of organic carbon, contributions to alkalinity from anaerobic metabolisms, and bioturbation fundamentally control the carbonate chemistry of the environments in which crystal fans would nucleate and grow and form the foundation for our model of the sediment-water interface.

#### 4.3.1 Modeling methods

We constructed an explicit framework to evaluate the conditions that might hinder or promote the growth of seafloor crystal fans with a focus on the role of geobiological processes in the chemistry of the sediment-water interface. During carbonate precipitation, the growth rate ( $R$ ) can be related to saturation state ( $\Omega$ ) through the following rate equation:

$$R = k * [CaCO_3] * (\Omega - 1)^n \quad (4.1)$$

where  $k$  is the rate constant and  $n$  is the rate order and saturation state ( $\Omega$ ) is defined as:

$$\Omega = \frac{\gamma Ca^{2+} * \gamma CO_3^{2-}}{K_{sp}} \quad (4.2)$$

where  $\gamma$  is the activity coefficient and  $K_{sp}$  is the solubility product. As  $\Omega$  increases, so does  $R$ . The potential mitigating effects of kinetic inhibitors on precipitation rate can be included in the rate equation with the coefficient  $k$ .

In order to quantify and formalize the possible biological controls on the sediment-

water interface chemistry, we used a mathematical model that is designed to explore the carbonate chemistry and saturation state of the sediment-water interface as a thermodynamic statistic to predict the behavior of carbonate precipitation and dissolution. The carbonate chemistry of the sediment-water interface can be understood as the difference between processes occurring in the water column versus those in the shallow sediments that either add or remove DIC and/or alkalinity in their respective environments. We can simulate the effect that the geobiological processes have on the  $\text{CaCO}_3$  saturation state of the interface with four boxes for dissolved inorganic carbon and alkalinity in the overlying water column ( $\text{DIC}_w$ ,  $\text{ALK}_w$ ) and in the shallow sediments ( $\text{DIC}_s$ ,  $\text{ALK}_s$ ), respectively, (Figure 4.1).

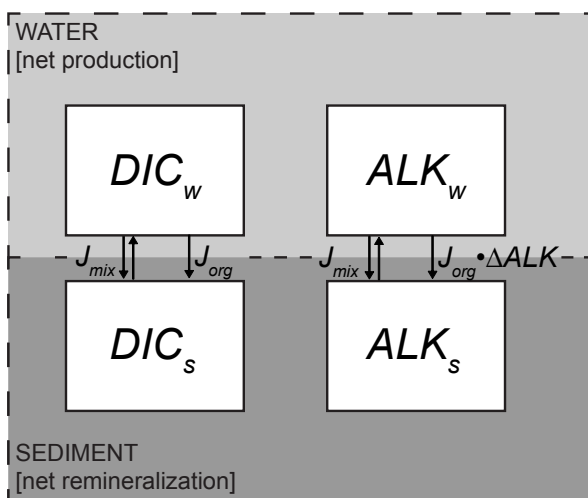


Figure 4.1: Topology of a mathematical model to examine the carbonate chemistry of the sediment-water interface model. DIC, dissolved inorganic carbon, ALK, alkalinity. The  $\text{DIC}_w$  and  $\text{ALK}_w$  are set to modern seawater values. The chemical work done on the sediment  $\text{DIC}_s$  and  $\text{ALK}_s$  is a function of the flux of organic material ( $J_{org}$ ) and the alkalinity input from different respiratory metabolisms.

We generate a flux of organic matter—from oxygenic photosynthesis and carbon fixation—to the sediment-water interface and force all remineralization to occur within sediments (Figure 4.1). We then vary the flux of organic matter and the dominant microbial respiration pathways responsible for organic matter remineralization. These simplifications approximate a variety of marine environments and demonstrate the importance of different microbial respiration pathways on the

chemistry at the interface. We overlook precipitation and dissolution feedbacks—which would make true changes in  $\Omega$  less than those predicted by the model—with the first-order goal of predicting thermodynamic favorability and likelihood of crystal fan development.

The four differential equations governing the box model are:

$$\frac{dDIC_w}{dt} = J_{mix} * ([DIC_s] - [DIC_w]) - J_{org} \quad (4.3)$$

$$\frac{dDIC_s}{dt} = J_{mix} * ([DIC_w] - [DIC_s]) + J_{org} \quad (4.4)$$

$$\frac{dALK_w}{dt} = J_{mix} * ([ALK_s] - [ALK_w]) - J_{org} * \Delta ALK \quad (4.5)$$

$$\frac{dALK_s}{dt} = J_{mix} * ([ALK_w] - [ALK_s]) + J_{org} * \Delta ALK \quad (4.6)$$

where  $J_{org}$  is the flux of organic material to the sediment-water interface and  $J_{mix}$  is the combined effect of advection and diffusion. These two processes would be accounted for differently in a time dependent model but because we are solving the model at steady state we have simplified their effect into a single term. A steady-state solution implies that removal from the sediment box is in equilibrium with the input. Solving equations 4.3-4.6 at steady state and assuming the  $J_{mix}$  term is equal for ALK and DIC yields:

$$J_{mix} = \frac{J_{org}}{[DIC_s] - [DIC_w]} = \frac{J_{org} * \Delta ALK}{(ALK_s) - (ALK_w)} \quad (4.7)$$

solving for  $ALK_s$  yields:

$$[ALK_s] = \Delta ALK * ([DIC_s] - [DIC_w]) + [ALK_w] \quad (4.8)$$

To simulate variable quantities of remineralized organic carbon in the sediment box we used the following expression:

$$[DIC_s] = [DIC_w] + [DIC_{remin}] \quad (4.9)$$

To solve the carbonate chemistry of this system, we adapted a version of the MATLAB solver from [44]. Constants were adjusted to those presented in Millero (2007) [45]. For boundary conditions (Table 4.2) we used values for  $[DIC_w]$ ,  $[ALK_w]$  and  $[Ca^{2+}]$  that reflect modern seawater, but the salient results hold over broad ranges of DIC and alkalinity. While  $[Ca^{2+}]$  has varied over geologic timescales, it is also likely true that  $[Ca^{2+}] \gg [CO_3^{2-}]$  over most of Earth history and thus gradients in  $\Omega$  were dependent on changes in  $[CO_3^{2-}]$  not  $[Ca^{2+}]$  [9]. At extreme end-member solutions of nearly zero  $[DIC_w]$ ,  $[ALK_w]$  and  $[Ca^{2+}]$  model outcomes are strongly affected. The large-scale commonalities in the carbonate producing environments throughout Earth history, however, suggest that these extreme conditions were never met by seawater [27, 1].

T	S	P	$[Ca^{2+}]$	$DIC_w$	$ALK_w$	$DIC_{remin}$	$\Delta ALK$
20 °C	35 ‰	1 atm	11 mmol kg <sup>-1</sup>	2100 μmol kg <sup>-1</sup>	2300 μmol equiv. kg <sup>-1</sup>	0:5:500 μmol kg <sup>-1</sup>	-1:0.1:9

Table 4.2: Boundary conditions for the mathematical model of sediment-water interface carbonate chemistry.

### 4.3.2 Modeling results

Modern marine environments demonstrate how inextricably linked the precipitation and dissolution of carbonate minerals are to the processes of organic carbon synthesis and remineralization. The dominant microbial respiration processes occurring in shallow sediments and at the sediment-water interface in the modern, however, have changed throughout Earth history [9, 25]. This is important because while respiration always adds DIC, anaerobic respiration pathways also contribute alkalinity and thus have a different effect on  $\Omega$  than aerobic metabolisms (Table 4.3, Figure 4.2). Figure 4.2 illustrates the alkalinity produced for 10 μmol

kg-1 of organic matter respired to CO<sub>2</sub> for different respiration pathways— aerobic respiration, sulfate reduction, nitrate reduction, manganese reduction, iron reduction, methanogenesis and anaerobic oxidation of methane (AOM). The alkalinity contribution was calculated by balancing the stoichiometry of marine organic carbon, oxygen and hydrogen from Anderson (1995) but ignores the smaller effects of remineralizing nitrogen and phosphorous [46]. In this regard, the alkalinity contributions from these anaerobic metabolisms are further distinct from aerobic respiration. The anaerobic remineralization of nitrogen adds alkalinity because the organic nitrogen is transformed to ammonia but removes alkalinity in oxic settings as organic nitrogen is metabolized, in net, to nitrate (not commonly by the same organisms). Aerobic respiration actually removes a small amount of alkalinity for every mole of CO<sub>2</sub> respired because of nitrogen and phosphorous remineralization. Aerobic respiration and methanogenesis are respiration pathways that result in >1 mol equivalent alkalinity per mol of CO<sub>2</sub> and thus these respiration pathways decrease the carbonate saturation of pore waters (Table 4.3, Figure 4.2). Manganese reduction, iron reduction, the anaerobic oxidation of methane and sulfate reduction promote carbonate precipitation by boosting the carbonate saturation state of pore waters. The relative contribution to alkalinity per mol of CO<sub>2</sub> is referred to here as  $\Delta\text{ALK}$  and is shown by the slope of the vectors plotted in Figure 4.2. The resulting effect of these respiration pathways on  $\Omega_{\text{aragonite}}$  (contours) is consistent over a broad range of seawater chemistry, however note that at end-member compositions (either negligible DIC or Alkalinity) the effect on  $\Omega$  would be different.

The steady-state solutions for this simple two-box model are a function of the flux of organic matter to the sediment-water interface and the effect of different microbial respiration pathways on alkalinity per mol CO<sub>2</sub> ( $\Delta\text{ALK}$ ). Results are presented as pH and  $\Omega_{\text{aragonite}}$  of the sediment box (Figure 4.3A,B). While each respiratory pathway listed earlier has a specific  $\Delta\text{ALK}$  contribution, we explored a continuum in  $\Delta\text{ALK}$  (-1–9) to approximate the combined effect of multiple respiratory pathways due to the common limitation of electron acceptors in organic-rich

REACTION	STOICHIOMETRY	$\Delta$ DIC	$\Delta$ ALK	pH	
aerobic respiration	$4 \text{ C}_{106}\text{H}_{175}\text{O}_{42} + 515 \text{ O}_2 \rightarrow 424 \text{ CO}_2 + 350 \text{ H}_2\text{O}$	1	0	5.18	
denitrification	$2 \text{ C}_{106}\text{H}_{175}\text{O}_{42} + 206 \text{ NO}_3^- + 206 \text{ H}^+ \rightarrow 212 \text{ CO}_2 + 103 \text{ N}_2 + 278 \text{ H}_2\text{O}$	1	1.0	6.78	
manganese reduction	$2 \text{ C}_{106}\text{H}_{175}\text{O}_{42} + 515 \text{ MnO}_2 + 1030 \text{ H}^+ \rightarrow 212 \text{ CO}_2 + 515 \text{ Mn}^{2+} + 690 \text{ H}_2\text{O}$	1	4.9	+	
iron reduction	$2 \text{ C}_{106}\text{H}_{175}\text{O}_{42} + 515 \text{ Fe}_2\text{O}_3 + 2060 \text{ H}^+ \rightarrow 212 \text{ CO}_2 + 1030 \text{ Fe}^{2+} + 1205 \text{ H}_2\text{O}$	1	9.7	+	
sulfate reduction	$8 \text{ C}_{106}\text{H}_{175}\text{O}_{42} + 515 \text{ SO}_4^{2-} + 1030 \text{ H}^+ \rightarrow 848 \text{ CO}_2 + 515 \text{ H}_2\text{S} + 700 \text{ H}_2\text{O}$	1	1.2	6.72	
methanogenesis	$8 \text{ C}_{106}\text{H}_{175}\text{O}_{42} + 330 \text{ H}_2\text{O} \rightarrow 333 \text{ CO}_2 + 515 \text{ CH}_4$	1	0	5.56	
AOM	$8 \text{ C}_{106}\text{H}_{175}\text{O}_{42} + 515 \text{ SO}_4^{2-} + 1030 \text{ H}^+ \rightarrow 848 \text{ CO}_2 + 515 \text{ H}_2\text{S} + 700 \text{ H}_2\text{O}$	1	1.2	7.88	
sulfide oxidation	$1 \text{ H}_2\text{S} + 2 \text{ O}_2 \rightarrow \text{SO}_4^{2-} + 2 \text{ H}^+$	0	-2	-	
iron oxidation	$4 \text{ Fe}^{2+} + 4 \text{ H}_2\text{O} + \text{O}_2 \rightarrow 2 \text{ Fe}_2\text{O}_3 + 8 \text{ H}^+$	0	-8	-	

Table 4.3: Different respiratory metabolisms have unique effects on solution carbonate chemistry. The redox reactions were balanced below using the stoichiometry  $\text{C}_{106}\text{H}_{175}\text{O}_{42}$  (Anderson1995) to approximate the average redox composition of marine organic matter. The  $\Delta$ ALK term is the change in alkalinity per mol of organic carbon turned to  $\text{CO}_2$  and was calculated for each reaction as a function of the principal components at the  $\text{CO}_2$  equivalence point. The pH column indicates the pH midpoint, below which the reaction will result in a pH increase and above which the reaction will result in a pH decrease. The colors designated for each respiration pathway are the color of the respective arrow in Figure 4.2.

column 5 from [47]

sediments. The dark blue regions represent the sediment box when  $\Omega_{\text{aragonite}}$  is less than one (Figure 4.3B). These undersaturated environments would promote dissolution of aragonite and are similar to the shallow sediments in the modern ocean.

These calculations demonstrate how the chemistry of the sediment-water interface can deviate strongly from seawater due to expected geobiological processes. Interestingly, these relationships show two mutually exclusive paths that result in favorable chemistry for crystal fan formation. One, in anoxic environments with anaerobic metabolisms above  $\Delta$ ALK = 0.8,  $\Omega_{\text{aragonite}}$  of the sediment box does not drop below one, even with high rates of organic matter delivery ( $500 \mu\text{mol kg}^{-1}$ ). And two, if organic matter delivery is sufficiently low ( $< 50 \mu\text{mol kg}^{-1}$ ) the sediments do not become undersaturated even when  $\Delta$ ALK is equal to -1 (Figure 4.3).

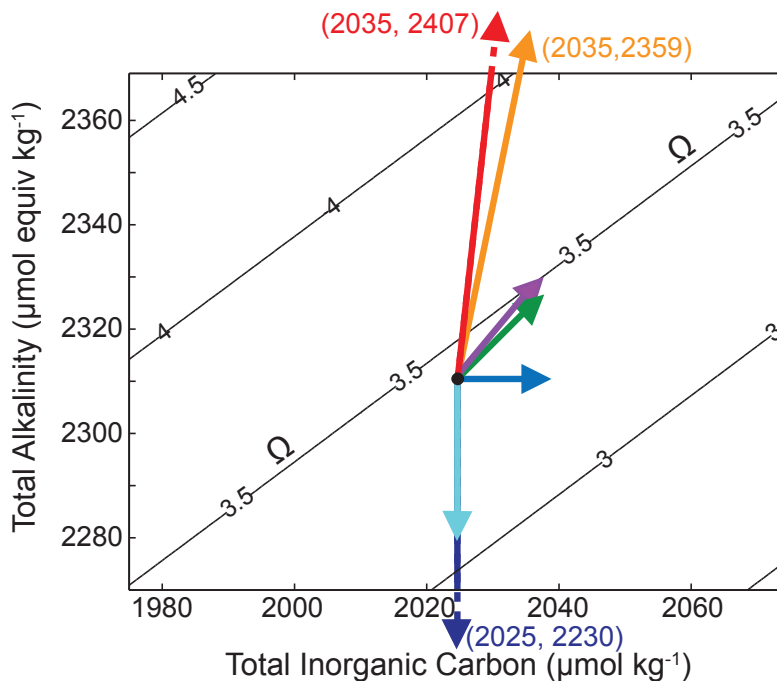


Figure 4.2: Effect of different respiratory metabolisms on dissolved inorganic carbon (DIC), alkalinity, and  $\Omega_{aragonite}$  in a hypothetical environment when  $10 \mu\text{mol kg}^{-1}$  organic carbon is respired. The plot shows contours of equal  $\Omega_{aragonite}$  as a function of DIC and total alkalinity. The different colored vectors describe specific redox reactions shown in Table 4.3.

#### 4.4 Examples from the sedimentary record

Guided by the results of the mathematical descriptions of sediment-water interface chemistry, we can examine examples of crystal fans from the rock record for evidence that the two solutions might have been influential in driving seafloor carbonate precipitation. Evidence of microbially mediated precipitation via anaerobic respiration pathways might include: (1) a carbon isotopic composition  $^{13}\text{C}$ -depleted relative to coeval seawater due to local organic respiration, (2) reduced authigenic minerals such as pyrite produced in close association with the precipitates, or (3) reduced metals incorporated into the carbonate structure such as  $\text{Fe}^{2+}$  and  $\text{Mn}^{2+}$ . Whereas precipitation on surfaces with low organic matter delivery to the sediments might include: (1) low TOC concentrations in the interval with crystal fans, (2) incompletely reduced electron acceptors such as iron or manganese oxides, or (3) a lack of reduced minerals like pyrite.

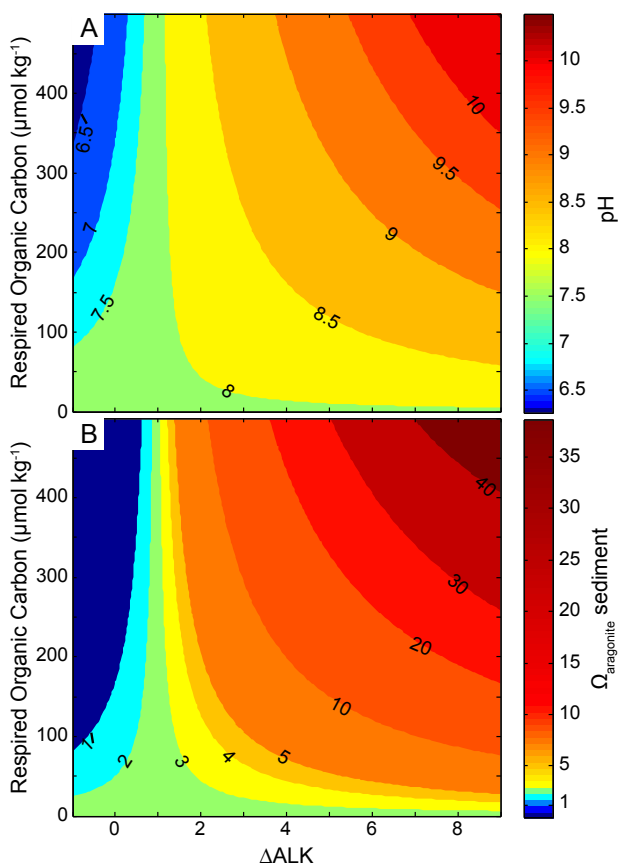


Figure 4.3: Results of the carbonate chemistry model, solved at steady state, in terms of pH (A) and  $\Omega_{\text{aragonite}}$  (B) of the sediment box. For this calculation, the water box has a fixed pH of 7.9 and  $\Omega_{\text{aragonite}}$  of 2.36. The results indicate both pH and  $\Omega_{\text{aragonite}}$  will drop for all  $f_{org}$  (0–500  $\mu\text{mol kg}^{-1}$ ) and  $\Delta\text{ALK} < 1$ . For all  $\Delta\text{ALK}$  and  $f_{org} < 50 \mu\text{mol kg}^{-1}$ ,  $\Omega_{\text{aragonite}}$  remains  $> 1$ . Additionally,  $\Delta\text{ALK} > \sim 2$  will result in strongly supersaturated sediment pore fluids.

calculations adapted from [44]

We examined two examples of crystal fans from the Proterozoic based on these predictions, the Beechey Formation (Figure 4.4) and the Rainstorm Member of the Johnnie Formation (Figure 4.5). Both examples are intriguing because of their close association with iron-rich accessory minerals [48, 49, 50].

#### 4.4.1 Petrographic, spectroscopic and isotopic methods

To better understand the petrogenesis of the Beechey Formation and Johnnie Formation crystal fans, we used a variety of high-resolution in situ methods including

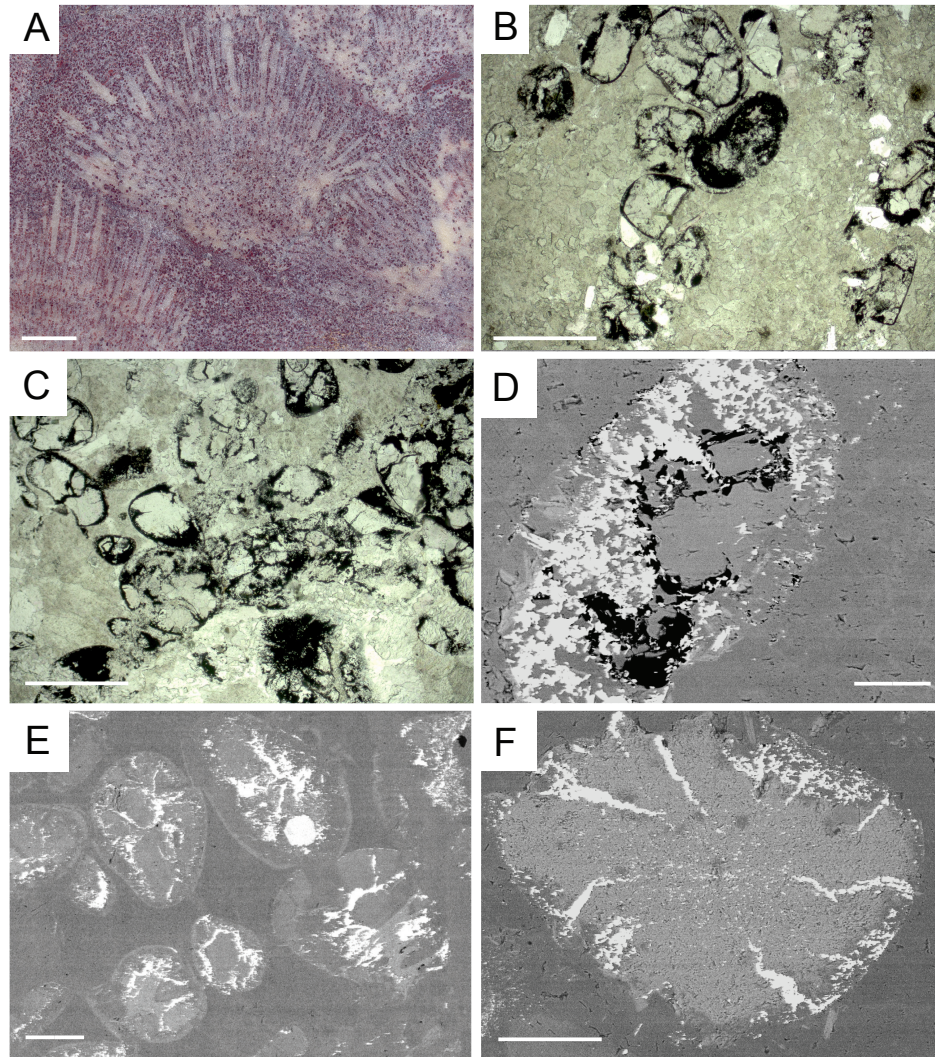


Figure 4.4: Paleoproterozoic Beechey Formation, NWT. A) Aragonite pseudomorphs display a radiating fanning morphology. Scale bar is 1 cm. B–C) Photomicrographs of the linear aragonite pseudomorphs with grains infilling around them. The opaque coatings are hematite and chert. Scale bars are 500  $\mu\text{m}$ . D) SEM image of a single grain composed mostly of hematite (highest backscatter) and silica (intermingled low backscatter). The angular clasts in the center of the grain are dolomite. Scale bar is 40  $\mu\text{m}$ . E) SEM image of grains of mixed mineralogy infilling around the aragonite pseudomorphs. The mineral with high backscatter is hematite and one round apatite grain, the mineral with medium backscatter is an illite-like clay mineral (in weight %  $\sim 1\text{--}2\%$  Mg, 14.5% Al, 25.5% Si, 9% K, 3–4% Fe) and the low backscatter matrix is dolomite. Scale bar is 200  $\mu\text{m}$ . F) SEM image of a single grain with hematite (high backscatter) filling in cracks within clay mineral. Scale bar is 100  $\mu\text{m}$ .

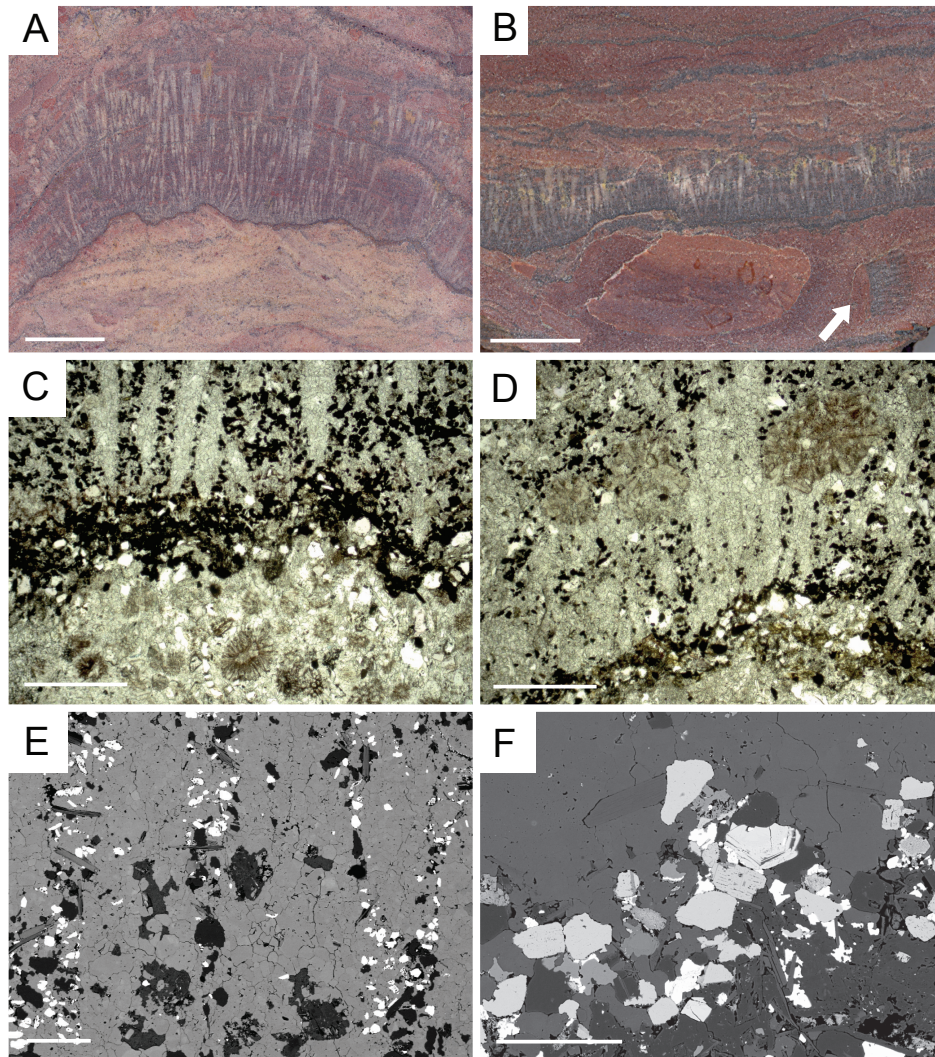


Figure 4.5: Rainstorm Member of the Ediacaran Johnnie Formation, Death Valley region, United States A–B) Aragonite pseudomorphs showing near-vertical growth with a fanning morphology near the nucleation point. Note the rip-up clast containing aragonite crystal fan pseudomorphs (arrow) in B. Scale bars are 1 cm. C–D) Photomicrographs of aragonite pseudomorphs with quartz grains (white), opaque hematite and iron-titanium oxide grains, and ooids (below crystal fan nucleation horizon). Note the three ooids stopping the growth of the crystal fans in D. Scale bars are 500  $\mu\text{m}$ . E–F) SEM images of aragonite pseudomorphs (now calcite) with detrital grains infilling around the blades. Accessory minerals include muscovite (light grey), quartz (black), hematite, iron-titanium oxides, barite (white), zircon (light grey-center of F), and rutile (white). Scale bars are 200  $\mu\text{m}$  and 100  $\mu\text{m}$ , respectively.

transmitted and reflected light microscopy, scanning electron microscopy (SEM), energy dispersive spectroscopy (EDS), micro x-ray fluorescence ( $\mu$ XRF), wavelength dispersive spectroscopy elemental analysis using an electron microprobe, Raman spectroscopy, and electron backscatter diffraction (EBSD). These techniques provide information on the crystallography and diagenesis of the carbonate fabrics, but also help highlight the chemistry and textures of accessory phases and surrounding sediments, which provide important insights into the chemical and physical environments of the sediment-water interface during at the time of crystal fan precipitation. The accumulation of authigenic minerals (e.g., apatite, barite and iron-bearing minerals) can provide additional information about relative crystal fan growth rates, bottom water chemistry, organic diagenesis, and important metabolic processes that once operated at the sediment-water interface (e.g., [51]). To fully assess the character of the crystal fans and surrounding sediments we designed the following workflow: (1) petrography of representative thin sections, (2) elemental mapping at a thin-section scale using  $\mu$ XRF, (3) mineralogical identification using Raman spectroscopy, (4) semiquantitative elemental spot analysis and elemental mapping with EDS using the ZEISS 1550 VP Field Emission Scanning Electron Microscope (SEM), and (5) quantitative elemental spot analysis and elemental mapping using the JEOL JXA-8200 Electron Microprobe on the various carbonate components to assess trace metal variations between textures and on iron oxides to estimate valence state. For all quantitative results, the accelerating voltage was 15 kV, the beam current was 20 nA, and the beam size was 1  $\mu$ m. The CITZAF method was used for matrix correction. Sample standards for the five chemical elements analyzed, included: calcite for Ca, dolomite for Mg, siderite for Fe, rhodochrosite for Mn, strontianite for Sr, and anhydrite for S. Ca had an average detection limit of 170 ppm, Mg-270 ppm, Fe-320 ppm, Mn-290 ppm, Sr-490 ppm, and S-90 ppm.

Isotopic analysis of the crystal fan pseudomorphs and surrounding matrix for the Beechey Formation was conducted at University of Michigan Stable Isotope Laboratory because no published isotopic data existed prior to this study. Ten

mg of carbonate samples were weighed into stainless steel boats and heated to 200°C under vacuum for one hour prior to reaction. Samples were then reacted in individual borosilicate reaction vessels at 77°C for 12 minutes with 4 drops of anhydrous phosphoric acid on a ThermoFinnigan MAT Kiel IV device coupled to a ThermoFinnigan MAT 253 triple collector isotope ratio mass spectrometer. Two standards were analyzed in conjunction with the samples, NBS 18 and NBS 19 and measured precision is maintained at better than 0.1‰ for both carbon and oxygen isotopic compositions.

Electron backscatter diffraction (EBSD) provides a useful technique for assessing the mineralogy and replacement texture of the crystal fan samples on the SEM. Seafloor crystal fans are thought to have had an original mineralogy composed of aragonite based on the acicular morphology, feathery or square terminations, hexagonal cross sections and botryoidal fanning growth habits [10, 52, 2, 11]. Observations of crystal fans in the record reconstruct the primary texture to have consisted of acicular crystals of aragonite, bundled together to form crystal aggregates with blunt terminations. The linear, radiating fabric elements that delineate the crystal fans represent the neomorphic equivalent of these crystal bundles [10, 53, 54, 55]. In all known examples, primary aragonite was replaced by a calcite or dolomite mosaic texture, or occasionally silica [10, 11]. The mosaic replacement texture varies, and can be equant, interlocking, or elongated, but importantly, the crystals composing the mosaic are not optically oriented [52, 11].

These observations provide the basis for a method of assaying the original mineralogy and crystal form, now replaced, by mapping the optical orientation of these replacement mosaics using the electron backscatter detector (EBSD) on the SEM to obtain diffraction data (for mosaic maps generated with EBSD see Figure 4.6) [56]. The expected random orientation of the mosaic replacement pattern is seen in the Johnnie Formation example where the map area is within a single crystal fan pseudomorph (Figure 4.6A,B). In contrast, an example of a putative aragonite crystal fan occurrence documented from the Early Triassic Union Wash Formation, Inyo Mountains, California—one of the youngest observed

in the sedimentary record—does not reveal the expected random grain orientations in the mosaic where the map area covers multiple blades suggesting a primary calcite mineralogy (Figure 4.6C,D) [57, 22, 58, 59].

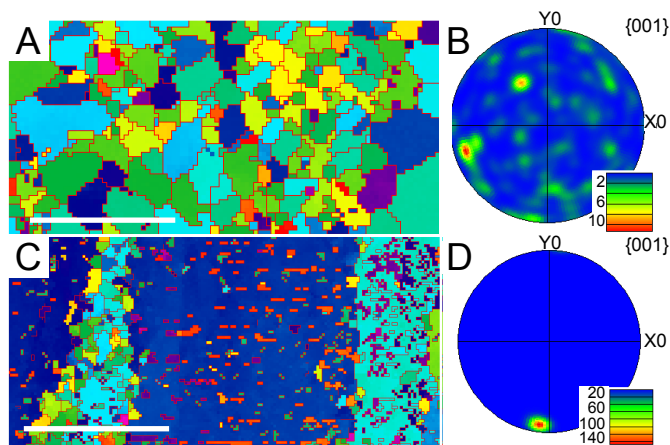


Figure 4.6: SEM mosaic images of the Johnnie Formation and the Union Wash Formation made using the electron backscatter detector (EBSD). A) Crystal orientation map within a single aragonite pseudomorph from the Johnnie Formation ( $3 \mu\text{m}$  window). This example shows a calcite mosaic fabric has replaced the original aragonite. Scale bar is  $100 \mu\text{m}$ . B) C-axis pole figure of the crystal orientation map indicates no preferential orientation of the calcite mosaic. C) Crystal orientation map through three fibrous calcite blades from the Union Wash Formation showing no replacement mosaic ( $10 \mu\text{m}$  window). Scale bar is  $500 \mu\text{m}$ . D) C-axis pole figure of the crystal orientation maps indicate the calcite blades are oriented parallel to the c-axis indicating length-fast calcite.

#### 4.4.2 Paleoproterozoic Beechey Formation, NW Territories, Canada

The Paleoproterozoic Beechey Formation is part of the Bear Creek Group deposited in the Kilohigok Basin  $\sim 1.9 \text{ Ga}$  [60]. The Bear Creek Group is contemporaneous with the passive margin deposits preserved in the Wompay Orogen but records a unique tectonic history. The lower units of the Bear Creek Group document the developing Thelon Tectonic Zone, which caused both flexural subsidence in the foredeep and arching in the nearshore environments of the foreland basin [60]. The Bear Creek Group overlies the drowned Kimerot Platform and records rapid subsidence followed by infilling of the foreland basin. The Beechey Formation, largely comprised of shallow marine shelf siliciclastics, overlies deeper water submarine fan deposits of the Rifle Formation [60]. The crystal fans de-

veloped at the sequence boundary that marks the division between the Rifle and Beechey Formations [48].

The aragonite pseudomorphs form radial-fanning botryoids that grew as large as 10 cm wide and 30 cm tall. The pseudomorphs towards the center of the botryoids are narrower and increase in thickness and length towards the outside of the botryoids. The botryoids grew together to form deposits 1.5 m thick that extend laterally up to 40 km [48]. Iron-coated aggregate grains of chert, iron-rich clay and carbonate fill in between and highlight the carbonate crystal fan pseudomorphs (Figure 4.4). The mineralogy of the grains infilling around the crystal fans help informs the sedimentary geochemistry of this environment.  $\mu$ XRF mapping was completed on a thin-section sample of the Beechey Formation crystal fans using a 100  $\mu$ m resolution for Ca, Mg, Al, Si, S, K, Fe, Ti, Mn, and Sr. Ca, Fe and Si elemental distribution maps of the Beechey crystal fans are shown in Figures 7AC. The elemental distribution of calcium clearly highlights the individual carbonate pseudomorphs within two botryoidal fans (Figure 4.7A). The elemental distribution of iron shows essentially the negative image, faintly outlining the individual pseudomorphs as well as the space between the two botryoids (Figure 4.7B). Finally the silicon map shows three quartz veins crosscutting the two botryoids as well as clastic sediment fill between the crystal fan blades (Figure 4.7C).

Photomicrographs and SEM analysis of individual authigenic grains that accumulated around the pseudomorphs reveals interesting morphologies (Figure 4.4B–F). Most grains are round to sub-spherical, and, based on EDS analysis, are aggregates with an authigenic iron-silica coating. The coatings cement dolomite, quartz and an illite-like clay mineral composed primarily of Al, Si, K, Fe and Mg (Figure 4.4D–F). In addition to grain coatings, the iron-silica precipitates cement the interiors of the grains (Figure 4.4D–E) and fill internal syneresis cracks (Figure 4.4F). The interlocking iron-silica precipitate texture is best seen in Figure 4.4D. These grains are similar in texture and composition to those known from Paleoproterozoic-age circum-Superior granular iron formations [61, 62, 63, 64].

Quantitative trace metal analysis (Ca, Mg, Sr, Fe, Mn and S) of five differ-

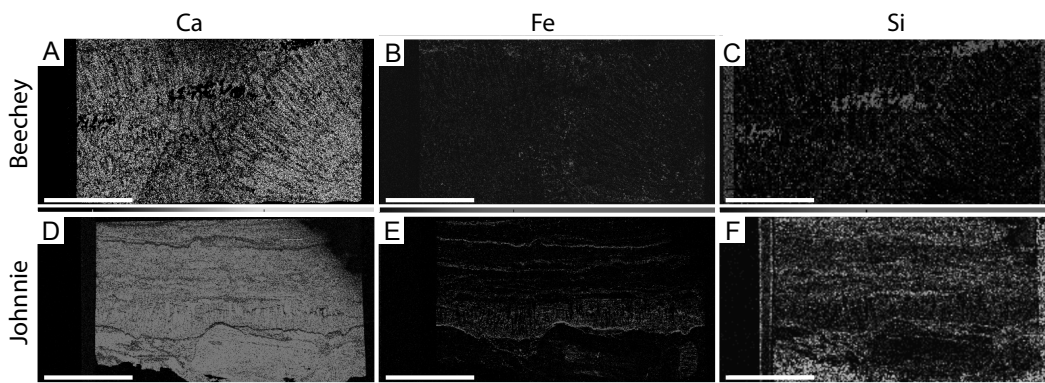


Figure 4.7:  $\mu$ XRF maps of thin sections of the Beechey Formation (A–C) and Johnnie Formation (D–F). Images are in grey scale to bring out contrast, where lighter shades correspond to an increasing rate of detector counts. A) Ca map with a range from 0 to 734 counts per second. B) Fe map with a range from 0 to 838 counts per second. C) Si map with a range from 0 to 524 counts per second. D) Ca map with a range from 0 to 1101 counts per second. E) Fe map with a range from 0 to 655 counts per second. F) Si map with a range from 0 to 498 counts per second. Scale bar in all images is 21  $\mu$ m.

ent carbonate phases were analyzed using an electron microprobe. A backscatter image and elemental abundance maps of Mg, Fe and Mn of a single crystal fan blade highlighted by iron oxide coated grains is shown in Figures 8AD. Quantitative spot analyses of five distinguishable fabrics were analyzed to calibrate the intensity maps—dark crystal fan pseudomorph (dcf), medium intensity cements in the crystal fan pseudomorph (mcf), light intensity cements in the crystal fan pseudomorph (lcf), light intensity dolomite within aggregate grains (lc), and dark intensity carbonate associated with the iron oxide coatings on the aggregate grains (dc) (Figure 4.8A). The three generations of pseudomorph replacement textures are appreciably distinct with clear zonation in the medium and light cement phases suggesting slow replacement and reprecipitation of the crystal fan blades. The different phases have strikingly different trace metal incorporation, particularly in iron and manganese. The medium zoned crystal fan cement shows the highest manganese incorporation (avg. 4300 ppm Mn), whereas the lightest, final cement phase is highest in iron (avg. 5.2 weight % Fe). The other phases have similar manganese concentrations ( $\sim$  2000 ppm Mn). The dolomite in the aggregate grains

is similarly high in iron (avg. 5 weight % Fe) but the dolomite most closely associated with the iron oxides rimming the clasts is significantly lower in iron (avg. 2.4 weight % Fe). These data suggest substantial amounts of reduced iron and manganese in the precipitating fluids, both early (as in the case of the dolomite within the aggregate grains) and later during diagenesis and replacement of the aragonite crystal fans. Metal enrichments this substantial likely record the effects of dissimilarity metal oxide reduction in this environment, however, the possibility of later diagenetic additions makes this difficult to conclude with certainty. Isotopic analysis of the crystal fans and surrounding matrix—a combination of cements and aggregate grains of carbonate, chert, clays and iron oxides—was conducted to help constrain the degree to which the crystal fans incorporated light remineralized carbon during their precipitation. The crystal fans ( $\delta^{13}\text{C}_{VPDB}$  -0.16, 0.42, 0.89‰,  $\delta^{18}\text{O}_{VPDB}$  -10.6, -9.47, -9.43‰) and surrounding matrix ( $\delta^{13}\text{C}_{VPDB}$  0.02, 0.40, 0.79‰,  $\delta^{18}\text{O}_{VPDB}$  -10.69, -9.11, -10.06‰) show little isotopic difference between the two and neither component is substantially  $^{13}\text{C}$ -depleted, though the O isotope ratios suggest some post-depositional resetting. This is different than the C isotopic systematics commonly observed in iron formation carbonate minerals [65] and suggests that little microbial work was required on this system to promote carbonate precipitation, perhaps due to a higher amount of DIC in seawater or a smaller biological pump, or both [66, 65].

#### 4.4.3 Neoproterozoic Johnnie Formation, Death Valley region, USA

The Ediacaran-aged Johnnie Formation hosts crystal fans in the Rainstorm Member, in a sequence of pink and grey limestone beds 10 - 20 m thick [49, 50]. The Rainstorm Member crystal fans are not associated with the Marinoan cap carbonate sequence, which in the Death Valley region is captured within the Noonday Formation [67, 68, 69]. This occurrence is one of just a few examples of aragonite seafloor crystal fans in strata between the Marinoan-age cap carbonates and the seafloor fans of Lower Triassic strata, though crystal fans reported from the Katak-

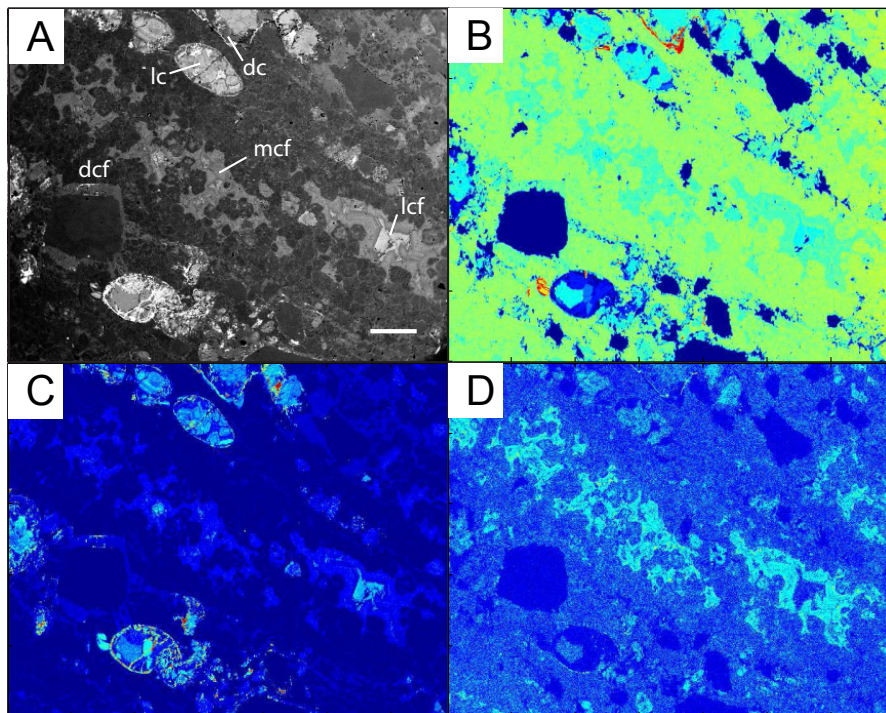


Figure 4.8: Electron microprobe maps of trace elements in the carbonate phases of the Beechey Formation. A) Backscatter image of a single crystal fan pseudomorph highlighted by accessory grains. Five carbonate textures were identified (dark crystal fan pseudomorph (dcf), medium intensity cements in the crystal fan pseudomorph (mcf), light intensity cements in the crystal fan pseudomorph (lcf), light intensity dolomite within aggregate grains (lc), dark intensity carbonate associated with the iron oxide coatings on the aggregate grains (dc)). Scale bar is 310  $\mu\text{m}$ . BD) Intensity maps of Mg, Fe and Mn, respectively. The corresponding quantitative measurements for the different carbonate phases can be found in Table 4.4.

turuk Dolomite in Alaska might be of similar age (Table 4.1) [19]. The Rainstorm fans coincide with the nadir of a major middle Ediacaran carbon isotope anomaly ( $-11\text{‰}$   $\delta^{13}\text{C}_{VPDB}$ ) termed the Shuram excursion (e.g., [70, 50, 71, 72, 73]).

The crystal fans appear grey in outcrop, forming laterally extensive sheets of variable thickness (1–20 cm), and are currently only observed at localities within the southern Nopah Range. The seafloor fans are interbedded with pink intraclast conglomerate and oolitic grainstone that include clasts of crystal fans lithologies (Figure 4.5A–B). The individual pseudomorphs are near vertical with fanning apparent near the points of nucleation (Figure 4.5A–B). The fans nucleate from horizons rich in iron-minerals, and the individual blades are surrounded by iron

phases [49, 50].  $\mu$ XRF elemental mapping was completed on the Rainstorm Member crystal fans at 100  $\mu$ m resolution for Ca, Mg, Al, Si, S, K, Fe, Ti, Mn, and Sr. We observed that the horizon from which crystal fans nucleated has high iron concentrations compared to surrounding sediments, though other iron-rich laminae did not nucleate fans (Figure 4.7E). EDS and Raman spectroscopy measurements were made to determine the mineralogy of the associated sediment. Nucleation horizons are comprised of a striking diversity of minerals, including calcite, dolomite, quartz, hematite, rutile and anatase (both titanium oxides), ilmenite, muscovite, biotite, zircon, apatite, barite and monazite (Figure 4.5). The hematite and titanium oxides are the most abundant minerals after calcite and quartz. The diversity of iron and titanium oxide minerals, their morphologies, relative density, and solubility characteristics altogether suggest a detrital origin (Figure 4.5C-F). Sedimentation of both hematite and iron-titanium oxide phases persist above the crystal fan nucleation horizon and infill around the crystal fans (Figure 4.5C-F). We used the relative backscatter contrast on the SEM to estimate and compare the mineral abundances of the intraclast ooid grainstone versus the crystal fan interval. The intraclast ooid grainstone is  $\sim$  75% calcite, 20% quartz, and 5% minerals with high backscatter (i.e., hematite). The crystal fan region surveyed is  $\sim$  70% calcite, 10% dolomite, 10% quartz, and 10% minerals with high backscatter. Trace iron phases that pigment the pink intraclast-rich limestones are concentrated within and around detrital carbonate phases like ooids and intraclasts (Figure 4.5A,B), whereas the iron-rich phases associated with the crystal fans are found in sub-spherical hematite grains. The mineral lamina that the crystal fans nucleate from could mark dissolution events that concentrated recalcitrant minerals, however, we do not favor this model because quartz is not enriched at these horizons (Figure 4.7F). Consequently, dissolution driven precipitation (like that seen in Paleozoic hardgrounds, e.g., [74]) is unlikely. The hematite grains remain an important component of the sediment infilling around the crystal fans and are not just in the lamina from which crystal fan growth initiated.

A backscatter image and elemental abundance maps of Mg, Fe and Mn of a

crystal fan horizon highlighted by iron and titanium oxides is shown in Figures 9A–D. Quantitative trace metal analyses (Ca, Mg, Sr, Fe, Mn and S) of four distinguishable carbonate fabrics were completed to calibrate the intensity maps—matrix cement below the crystal fan interval (pc), ooids below the crystal fan interval (oo), crystal fan pseudomorphs (cf), and cement filling around the crystal fan pseudomorphs and between iron oxide grains, etc. (cfc) (Figure 4.9A). The crystal fan pseudomorphs had the lowest concentration of iron and the highest of manganese (avg. 460 ppm Fe, avg. 680 ppm Mn, max. 3580 ppm Mn). In contrast, the ooids were highest in iron (avg. 6400 ppm Fe, max 4.2 weight % Fe) although some of this signal is probably carried by finely disseminated iron oxides observed as small, micron-scale high-backscatter inclusions occasionally interspersed in these coated grains. The cements surrounding the crystal fans were distinct from the fans themselves and were also high in iron (avg. 4140 ppm Fe, max. 3.2 weight % Fe). These results suggest that some metal reduction was likely occurring in the shallow sediments, however, a significant portion of the metals remain in higher-valent oxides (including manganese) (Figure 4.9C-D). Additionally, there is no evidence of pyrite in these rocks suggesting sulfate reduction was not significant and organic matter inputs were relatively low. Altogether, these observations suggest minimal organic diagenesis and consequently little microbial work on the carbonate chemistry over environmental DIC. The lack of isotopic variability in the Johnnie Formation supports this, suggesting a well-mixed isotopic reservoir, most likely marine DIC [50].

## 4.5 Discussion

From the perspective of our mathematical framework there were several paths, in principle, to develop favorable chemical conditions for crystal fan growth at the sediment-water interface. One end-member solution depends on anoxic conditions and anaerobic respiration pathways that increase carbonate saturation state at the sediment-water interface. The other end-member solution describes a scenario

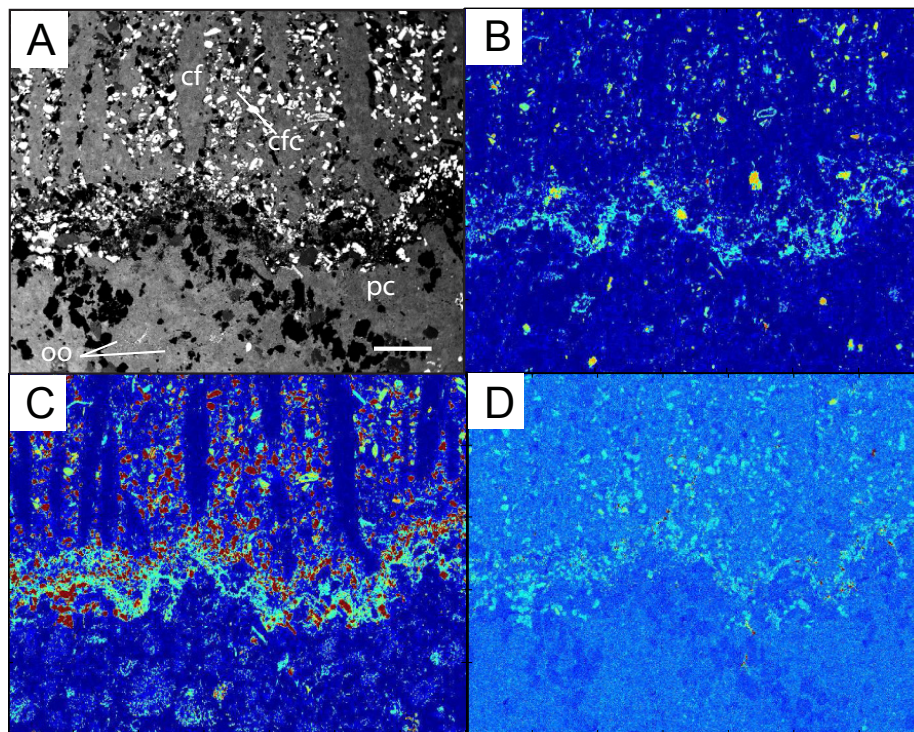


Figure 4.9: Electron microprobe maps of trace elements in the carbonate phases of the Johnnie Formation. A) Backscatter image of a crystal fan horizon highlighted by accessory grains. Four carbonate textures were identified: matrix cement below the crystal fan interval (pc), ooids below the crystal fan interval (oo), crystal fan pseudomorphs (cf), and cement filling around the crystal fan pseudomorphs and between iron oxide grains, etc. (cfc). Scale bar is 310  $\mu\text{m}$ . B-D) Intensity maps of Mg, Fe and Mn. The corresponding quantitative measurements for the different carbonate phases can be found in Table 4.4.

of low organic matter delivery to the sediments that results in little remineralized  $\text{CO}_2$  and little change to the carbonate chemistry in the shallow sediments, which—depending on the overlying seawater saturation state—could also promote seafloor crystal fan growth. These end-members provide a means to evaluate observations of seafloor crystal fans from the geologic record.

Our high-resolution petrographic analysis of two different Proterozoic occurrences of seafloor-precipitated crystal fans reveals distinct features that add insight into their origin. Both examples represent discrete intervals of seafloor precipitation—within hundreds to thousands of meters of surrounding stratigraphy—and both examples coincide with assemblages of accessory minerals and aggregates that shed light on the chemical and physical conditions that led to the seafloor

Carbonate Phase	Metal	Avg. %	Max. %	Min. %	Std. Dev.	# Analyses
Beechey DCF	Mg	13.635	15.087	11.242	0.486	65
Beechey MCF	Mg	12.370	14.179	10.048	0.783	64
Beechey LCF	Mg	10.673	12.708	9.594	0.699	26
Beechey LC	Mg	10.619	13.399	9.224	0.588	43
Beechey DC	Mg	12.654	14.294	10.157	1.046	21
Johnnie PC	Mg	0.201	0.525	0.081	0.097	50
Johnnie OO	Mg	0.232	0.411	0.115	0.067	31
Johnnie CF	Mg	0.195	0.413	0.01	0.087	66
Johnnie CFC	Mg	0.209	0.402	0.089	0.075	36
Beechey DCF	Fe	0.345	2.397	0.050	0.509	65
Beechey MCF	Fe	2.642	6.043	0.041	1.133	64
Beechey LCF	Fe	5.241	7.079	1.886	1.399	26
Beechey LC	Fe	5.088	6.235	1.692	0.739	43
Beechey DC	Fe	2.467	5.850	1.385	1.218	21
Johnnie PC	Fe	0.105	2.120	0.000	0.338	50
Johnnie OO	Fe	0.644	4.156	0.019	0.944	31
Johnnie CF	Fe	0.046	0.173	0.000	0.039	66
Johnnie CFC	Fe	0.414	3.298	0.050	0.692	36
Beechey DCF	Mn	0.191	0.621	0.100	0.071	65
Beechey MCF	Mn	0.431	0.986	0.100	0.176	64
Beechey LCF	Mn	0.192	0.351	0.109	0.073	26
Beechey LC	Mn	0.258	0.435	0.112	0.061	43
Beechey DC	Mn	0.178	0.353	0.105	0.061	21
Johnnie PC	Mn	0.026	0.112	0.000	0.026	50
Johnnie OO	Mn	0.041	0.130	0.000	0.030	31
Johnnie CF	Mn	0.068	0.358	0.000	0.084	66
Johnnie CFC	Mn	0.057	0.254	0.000	0.060	36

Table 4.4: Quantitative measurements of Mg, Fe and Mn from the five identified carbonate phases of the Beechey Formation (Figure 4.8) and four phases of the Johnnie Formation (Figure 4.9). The results are presented as average weight percent, maximum weight percent, minimum weight percent, standard deviation of measurements and # of spot analyses from each phase.

precipitation. Furthermore, examples from a literature review suggest other examples share similarities to the two deposits we studied.

The Beechey Formation crystal fans are notable for their co-occurrence with authigenic iron-silica minerals. These authigenic minerals formed and were deposited with the crystal fans during marine transgression, which is a common sequence stratigraphic occurrence for authigenic iron-mineral precipitation, as the transgressing shoreline floods rivers and slows the delivery of detrital sediment to offshore paleoenvironments [75, 76, 77]. In addition, the Beechey Formation crystal fans may have benefited from an environment wherein ferric iron served as an important electron acceptor for the respiration of organic matter. Iron reduction provides a strong alkalinity pump with a  $\Delta\text{ALK}$  of 9.7 promoting an increase in the carbonate saturation state of the sediments. This alkalinity boost was probably somewhat offset by iron cycling in this environment because of ferrous iron oxidation ( $\Delta\text{ALK}\sim-8$ ), though the net effect of this iron cycling was likely to turn ferric iron into mixed valence and ferrous iron silicates (e.g., [65]). Evidence that this was occurring can be inferred by the very high concentrations of reduced iron incorporated into the carbonates (3500 ppm - 5 weight %). A corresponding  $^{13}\text{C}$ -depletion in the crystal fan pseudomorphs from a remineralized organic component, however, is not readily apparent. That in mind, with the large alkalinity contribution from iron and manganese reduction, they improve the favorability of carbonate precipitation with smaller amounts of organic carbon. Caution is required because reduced metals are often incorporated into calcite and dolomite during burial diagenesis and recrystallization as diagenetic fluids are often reducing and carry enriched concentrations in these metals over seawater. Systematic differences between the different phases of carbonate (clasts in the aggregate grains vs. the multiple phases replacing the crystal fans), however, suggest that whole rock homogenization did not occur during diagenesis. Instead the crystal fans display a dolomite replacement sequence of the original aragonite beginning with an amorphous low iron, low manganese phase replacing the aragonite along the edges of the fan, an equant zoned high manganese dolomite replacing the interior of the

fans, and a final equant region of high iron dolomite in the core of the replacement cement. The development of incipient granular iron formation associated with the crystal fans suggests metal oxides used in respiration of the organic matter advected to this environment would have supplied alkalinity to buffer and/or increase the saturation state and promote crystal fan nucleation and growth. The crystal fans in the Beechey Formation sit on a hiatal surface that marks the sequence boundary between the Rifle and Beechey formations [48]. They were deposited during a transgression that resubmerged the shelf and are locally thickest where the condensed interval overlies the hiatal exposure surface. Sediment starvation associated with the condensed interval likely contributed to the favorable conditions leading to crystal fan formation [48]. This context suggests that sedimentation rate in the Proterozoic examples may be another important control on crystal fan occurrences as the Beechey Formation fans only appeared in the stratigraphy when sedimentation rates were lowest.

Our model results also provide helpful insights into the crystal fans that occur in the Johnnie Formation, which may have developed during an interval of reduced organic carbon flux to the seafloor and during a period of increased detrital metal oxide inputs. Like the Beechey Formation occurrence, these fans also co-occur with iron-bearing minerals. High-resolution microscopy shows that the iron is present primarily as ferric iron in accessory phases (mainly hematite but is also present in ilmenite and biotite). There are a few possibilities to explain the association between crystal fans and dense detrital accessory minerals. These include: (1) the dense minerals are a component of a wind-winnowed deposit (grain size between 10–100  $\mu\text{m}$ ), or (2) the heavy mineral lamina represent lag deposits where water winnowing removed less dense and finer grains. The seafloor was storm dominated, as evidenced by abundant rip-up intraclasts and hummocky cross-stratification, but in the maximum flooding interval, new sediment supply would have been diminished resulting in winnowing and density sorting of the grains. The mineral assemblage implies that the seafloor was oxic at the time of deposition with relatively little organic matter delivery to the seafloor. The

relative abundance of sedimentary organic matter can be inferred from the ferric iron-bearing secondary mineral assemblage because these phases are vulnerable to both early and late diagenetic destruction from the reducing power of organic matter (e.g., [78, 79, 51]). This inference is also supported by the presence of barite in this sample (Figure 4.6), which would have also been differentially susceptible to reductive dissolution. Empirically, these rocks contain exceedingly little residual organic carbon [70]. The isotopic composition of the crystal fan pseudomorphs and the surrounding matrix does suggest a large component of remineralized organic carbon, however, because the two phases not show systematic differences that would have resulted from organic matter respiration in shallow sediments or at the sediment-water interface, the depleted DIC source was likely well mixed [50]. Our model suggests that under aerobic conditions if the organic carbon input is  $< 50 \mu\text{mol kg}^{-1}$  or thereabouts, the sediment-water interface will remain supersaturated ( $\Omega_{\text{aragonite}} \sim 2.5$ ). Similar to the Beechey Formation crystal fans, the crystal fan beds in the Johnnie Formation also sit within a transgressive to high-stand systems tract that begins with deposition of the Johnnie oolite [49, 71]. The pink limestones that contain the crystal fan beds have been interpreted as the maximum flooding interval on the basis of their sedimentology, sequence stratigraphy, and carbon isotope systematics [49, 71, 72]. In this scenario, the crystal fans grew during a period of low background sedimentation corresponding to maximum flooding—a similar sequence stratigraphic context to the Beechey fans.

#### 4.5.1 Other examples from the rock record

Our analysis here helps contextualize additional crystal fan occurrences in the sedimentary record (Table 4.1). Prior to the rise of oxygenic photosynthesis, electron donors limited primary productivity [80, 51], and consequently organic fluxes to the sediment-water interface were likely substantially lower than today. This implies that the abundant crystal fan occurrences in Archean carbonate platforms, which are present across a range of shallow subtidal to supratidal paleoenvironmental settings [81], may have been due to a reduced flux of organic matter to the

seafloor, in addition to the general lack of aerobic respiratory metabolisms at that time [9]. After the rise of oxygen in Paleoproterozoic time, aerobic metabolisms would have begun to impact the carbonate chemistry of the seafloor. The continued occurrence of seafloor crystal fans well in Paleoproterozoic time, however, may reflect higher DIC concentrations in seawater due to the faint young sun and higher  $p\text{CO}_2$  [27, 82, 65]. Higher amounts of DIC would buffer the carbonate chemistry of the sediment-water interface and shallow sediments against undersaturation despite increasing amounts of organic delivery and aerobic respiration occurring on the seafloor and in surface sediments. As geological time wore on, and  $p\text{CO}_2$ , and DIC concentrations in the atmosphere and seawater decreased, promoting larger gradients in seawater saturation state and undersaturation of most seafloor settings [9], crystal fans were limited to times of carbon cycle perturbations.

Many Proterozoic crystal fans contain sedimentologic similarities to the Beechey and Johnnie formations crystal fans (Table 4.1). Multiple examples co-occur with detrital lag deposits (Cheshire Formation, Gaoyuzhuang Formation) and more specifically with hematite grains and coatings (Odjick-Rocknest Boundary, Maieberg Formation, Alwa Formation) although the details of the accessory sediments have not been examined in as much detail in these examples. Interestingly, several examples are also associated with pink, metal-rich limestones and the potential implication of this association bears further study (Teena Formation, Bambui Group, Maieberg Formation). Results from trace metal analysis of the Beechey and Johnnie Formations suggest these other examples of pink carbonates may also have substantially elevated concentrations of reduced Fe and/or Mn incorporated in the carbonate phase. The broad sequence stratigraphic context and low background sedimentation rate behavior is also observed for Neoproterozoic crystal fans that developed within the inferred interval of maximum flooding between the cap dolostones and overlying sediments during Marinoan post-glacial sea level rise (Odjick-Rocknest Boundary, Maieberg Formation, Mt. Doreen Formation, Bushmansklippe Formation, Hayhook Formation, Mirasol d'Oeste Formation, Ol Member, Tsagaan Oloom Formation, Katakturuk Formation, Shareza Formation

and Kokarkuyu Formation) [83, 14, 16, 17, 18, 19, 19]. In some instances this interval also contains barite precipitates (e.g., Mackenzie Mountains), which suggests the condensation of substantial amounts of time onto this horizon [8].

In thinking about the paucity of crystal fan examples in the Phanerozoic it is important to consider another important geobiological process that we do not explicitly address in our model, bioturbation by animals. Bioturbation can strongly affect the carbonate chemistry of the seafloor, by increasing mixing across the sediment-water interface and promoting aerobic respiration and reoxidation reactions [84]. Bioturbation is known from latest Ediacaran time to today, though there are clear secular changes in its intensity recorded by increasing ichnofabric indices [85] and shell bed thickness through time [86]. These trends probably played at least some role in the relative rarity of crystal fans in Phanerozoic sedimentary successions [5]. There are also feedbacks between bioturbation and redox processes that may have been important during times of crystal fan reappearance in the record. As seafloor anoxia becomes more prevalent in marine basins, burrowing intensity drops [43]. This will tend to set up strong vertical gradients as less oxygen is mixed into the sediments and more organic carbon is respired via anaerobic metabolisms, increasing  $\Omega$  and making conditions for crystal fan precipitation more favorable.

The crystal fans associated with the Permian-Triassic extinction and associated carbon cycle perturbations serve an informative example of these feedbacks and demonstrate that these sedimentary features could be globally important but related to general changes in the respiration of organic matter on the seafloor due to changing seawater redox budgets, rather than a long-term change in the saturation state of global seawater. The Permo-Triassic extinction was the most devastating mass extinction on record with the loss of  $\sim 55\%$  of marine invertebrate genera [7, 87]. Long-lived ecosystems were destroyed and seafloor bioturbation was greatly reduced with only small horizontal traces common [22]. 'Anachronistic' carbonate facies are well known from successions of this age [88]. These include an increase in aragonite cements filling cavities and forming on the seafloor in mid- to

late Permian reefs [89, 6], and, in many post-extinction sections, aragonite crystal fans appear directly on the seafloor or within cavities [21, 22, 23, 24]. Anoxia has been documented from Late Permian through Early Triassic oceans basins [90, 91]. Various observations imply widespread euxinic conditions, but more importantly, they demonstrate that sulfate reduction was an important process for remineralizing organic matter in anoxic sedimentary environments. In our model framework, these conditions (particularly the increase in anaerobic respiration, mainly through sulfate reduction, and reduction in bioturbation) would have facilitated the genesis of seafloor precipitates and crystal fans.

From the theoretical framework developed above it is clear, at least in principle, that seafloor crystal fans were influenced by geobiological processes operating on the seafloor. Intervals characterized by a higher frequency of crystal fan occurrences could reflect environmental changes global in scope, but perhaps due to other widespread phenomena like first-order changes in the magnitude of primary production and organic matter flux to the seafloor [92, 80] and the prevalence of bottom water anoxia [93], insofar as these phenomena would have impacted the carbonate chemistry of the sediment-water interface. Given these results, the dynamics of biological activity at the sediment-water interface has the ability to influence modes of carbonate precipitation and there is the potential for preserving evidence of such phenomena in the rock record.

## 4.6 Conclusions

Seafloor crystal fans represent a class of textures and mode of carbonate precipitation that is discrete in time. Substantial interest in these features exists with the goal of understanding their occurrence to help constrain secular changes in the fluid Earth carbon cycle. Our approach here was to build a mathematical framework for the role of microbial metabolism and organic carbon delivery on the sediment-water interface and to examine the petrography of two specific occurrences. From this work we can draw several conclusions:

1) Fundamental to understanding the petrogenesis of seafloor crystal fan textures is recognition that the nucleation of these features reflects the carbonate chemistry of the sediment-water interface. Geobiological processes involving physical mixing across this horizon (bioturbation) as well as redox reactions involved in the respiration of sedimentary organic carbon during diagenesis and reoxidation of the reduced products play critically important roles by adding or removing DIC and alkalinity, and altering the calcium carbonate saturation state. This is important because it is possible, in principle, that the problem of crystal fan origins can be divorced from surface seawater saturation states.

2) A model of the carbonate chemistry of the sediment-water interface as a function of important geobiological processes reveals two different end-member paths that produce favorable conditions for crystal fan genesis. In one organic matter is remineralized by anaerobic metabolisms that contribute both DIC and alkalinity, buffering or increasing the saturation state of the surface sediments. The second is characterized by little organic input to the sediments, contributing little DIC from respiration, and consequently maintaining favorable chemistry for crystal fan nucleation and growth from the sediment-water interface. These results suggest the hypothesis, supported by our high-resolution petrographic study of the Beechey and Johnnie formations, that not all crystal fans record the same geobiological phenomena.

3) Crystal fans from the Paleoproterozoic Beechey Formation likely reflect a sedimentary environment favorable for carbonate precipitation due to alkalinity sourced in part from iron reduction, evidenced by their co-occurrence with incipient iron formation and incorporation of high concentrations of reduced metals. Additionally, the sequence stratigraphic context of the Beechey fans suggest that they grew during a condensed interval, with low background sedimentation rates an important condition for growth.

4) Similarly, the crystal fans from the Rainstorm Member of the Neoproterozoic Johnnie Formation are associated with iron-rich detrital sediment and the trace element composition of the carbonate reflects elevated incorporation of reduced met-

als in the form of iron and manganese. However, much of the iron and manganese associated with the Rainstorm fans remains in the oxide phase, which points to low delivery of organic matter to the sediment-water interface with little aerobic organic diagenesis to hinder crystal fan precipitation and limited sulfate reduction. The crystal fans from the Rainstorm Member of the Neoproterozoic Johnnie Formation also occur during a maximum flooding interval suggesting preferential development during maxima in sedimentary accommodation.

## 4.7 Acknowledgements

We thank Sara Pruss, Jena Johnson, and an anonymous reviewer for insightful comments. Most analytical work was completed using facilities available in the Division of Geological and Planetary Sciences (GPS) at California Institute of Technology with assistance from Chi Ma, George Rossman and Andrew Matzen.  $\mu$ XRF analysis was completed at the Jet Propulsion Laboratory with assistance from Mark Anderson. Support from a Henshaw Fellowship (GPS) and a National Science Foundation Graduate Research Fellowship was provided to K. Bergmann. W. Fischer acknowledges support from the Agouron Institute and a David and Lucile Packard Fellowship for Science and Engineering.

## References

- [1] J.P. Grotzinger and N.P. James. Precambrian carbonates: evolution of understanding. volume Special Publication 67, pages 1–20. SEPM, 2000.
- [2] J.P. Grotzinger. Facies and evolution of Precambrian carbonate depositional systems - emergence of the modern platform archetype. *Controls on Carbonate Platform and Basin Development*, 44:79–106 399, 1989.
- [3] D.Y. Sumner and J.P. Grotzinger. Numerical modeling of ooid size and the problem of Neoproterozoic giant ooids. *Journal of Sedimentary Petrology*, 63(5):974–982, 1993.
- [4] D.Y. Sumner and J.P. Grotzinger. Herringbone calcite: Petrography and environmental significance. *Journal of Sedimentary Research*, 66(3):419–429, 1996.
- [5] J.P. Grotzinger and A.H. Knoll. Stromatolites in Precambrian carbonates: Evolutionary mileposts or environmental dipsticks? *Annual Review of Earth and Planetary Sciences*, 27:313–358, 1999.
- [6] J.P. Grotzinger, S.A. Bowring, B.Z. Saylor, and A.J. Kaufman. Biostratigraphic and geochronological constraints on early animal evolution. *Science*, 270(5236):598–604, 1995.
- [7] A.H. Knoll, R.K. Bambach, D.E. Canfield, and J.P. Grotzinger. Comparative Earth history and Late Permian mass extinction. *Science*, 273(5274):452–457, 1996.

- [8] P.F. Hoffman, G.P. Halverson, and J.P. Grotzinger. Are Proterozoic cap carbonates and isotopic excursions a record of gas hydrate destabilization following Earth's coldest intervals?: Comment. *Geology*, 30(3):286–287, 2002.
- [9] J.A. Higgins, W.W. Fischer, and D.P. Schrag. Oxygenation of the ocean and sediments: Consequences for the seafloor carbonate factory. *Earth and Planetary Science Letters*, 284(1-2):25–33, 2009.
- [10] J.P. Grotzinger and J.F. Read. Evidence for primary aragonite precipitation, Lower Proterozoic (1.9 Ga) Rocknest Dolomite, Wopmay Orogen, Northwest Canada. *Geology*, 11(12):710–713, 1983.
- [11] D.Y. Sumner. Microbial influences on local carbon isotopic ratios and their preservation in carbonate. *Astrobiology*, 1(1):57–70, 2000.
- [12] A.C. Allwood, J.P. Grotzinger, A.H. Knoll, I.W. Burch, M.S. Anderson, M.L. Coleman, and I. Kanik. Controls on development and diversity of Early Archean stromatolites. *Proceedings of the National Academy of Sciences of the United States of America*, 106(24):9548–9555, 2009.
- [13] W. Hegenberger. Stratigraphy and sedimentology of the Late Precambrian Witvlei and Nama Groups east of Windhoek. *Geological Survey of Namibia*, Memoir 17:82, 1993.
- [14] B.Z. Saylor, A.J. Kaufman, J.P. Grotzinger, and F. Urban. A composite reference section for terminal Proterozoic strata of southern Namibia. *Journal of Sedimentary Research*, 68(6):1223–1235, 1998.
- [15] J.G. Clough and R.K. Goldhammer. Evolution of the Neoproterozoic Katakaturuk dolomite ramp complex, northeastern Brooks Range, Alaska. volume Special Publication 67, pages 209–241. SEPM, 2000.
- [16] N.P. James, G.M. Narbonne, and T.K. Kyser. Late Neoproterozoic cap carbonates: Mackenzie Mountains, northwestern Canada: precipitation and

- global glacial meltdown. *Canadian Journal of Earth Sciences*, 38(8):1229–1262, 2001.
- [17] E. Font, A. Nedelec, R.I.F. Trindade, M. Macouin, and A. Charriere. Chemostratigraphy of the Neoproterozoic Mirassol d’Oeste cap dolostones (Mato Grosso, Brazil): An alternative model for Marinoan cap dolostone formation. *Earth and Planetary Science Letters*, 250(1-2):89–103, 2006.
- [18] P.F. Hoffman, G.P. Halverson, E.W. Domack, J.M. Husson, J.A. Higgins, and D.P. Schrag. Are basal Ediacaran (635 Ma) post-glacial ”cap dolostones” diachronous? *Earth and Planetary Science Letters*, 258(1-2):114–131, 2007.
- [19] F.A. Macdonald, D.S. Jones, and D.P. Schrag. Stratigraphic and tectonic implications of a newly discovered glacial diamictite-cap carbonate couplet in southwestern Mongolia. *Geology*, 37(2):123–126, 2009.
- [20] F.A. Macdonald, W.C. McClelland, D.P. Schrag, and W.P. Macdonald. Neoproterozoic glaciation on a carbonate platform margin in Arctic Alaska and the origin of the North Slope subterrane. *Geological Society of America Bulletin*, 121(3-4):448–473, 2009.
- [21] E. Heydari and J. Hassanzadeh. Deev Jahi model of the Permian-triassic boundary mass extinction: a case for gas hydrates as the main cause of biological crisis on Earth. *Sedimentary Geology*, 163(1-2):147–163, 2003.
- [22] S.B. Pruss, D.J. Bottjer, F.A. Corsetti, and A. Baud. A global marine sedimentary response to the end-Permian mass extinction: Examples from southern Turkey and the western United States. *Earth-Science Reviews*, 78(3-4):193–206, 2006.
- [23] A. Baud, S. Richoz, and S. Pruss. The lower Triassic anachronistic carbonate facies in space and time. *Global and Planetary Change*, 55(1-3):81–89, 2007.
- [24] J.L. Payne, D.J. Lehrmann, D. Follett, M. Seibel, L.R. Kump, A. Riccardi, D. Altiner, H. Sano, and J. Wei. Erosional truncation of uppermost Permian

- shallow-marine carbonates and implications for Permian-Triassic boundary events. *Geological Society of America Bulletin*, 119(7-8):771–784, 2007.
- [25] A.H. Knoll and W.W. Fischer. Skeletons and ocean chemistry: the long view. pages 67–82. Oxford University Press, New York, 2011.
- [26] J.P. Grotzinger. Geochemical model for Proterozoic stromatolite decline. *American Journal of Science*, 290A:80–103, 1990.
- [27] J.P. Grotzinger. New views of old carbonate sediments. *Geotimes*, 38:12–15, 1993.
- [28] L.M. Walter and E.A. Burton. Dissolution of recent platform carbonate sediments in marine pore fluids. *American Journal of Science*, 290(6):601–643, 1990.
- [29] L.M. Walter, S.A. Bischof, W.P. Patterson, and T.W. Lyons. Dissolution and recrystallization in modern shelf carbonates - evidence from pore-water and solid-phase chemistry. *Philosophical Transactions of the Royal Society of London Series a-Mathematical Physical and Engineering Sciences*, 344(1670):27–36, 1993.
- [30] X.P. Hu and D.J. Burdige. Enriched stable carbon isotopes in the pore waters of carbonate sediments dominated by seagrasses: Evidence for coupled carbonate dissolution and reprecipitation. *Geochimica Et Cosmochimica Acta*, 71(1):129–144, 2007.
- [31] X.P. Hu and D.J. Burdige. Shallow marine carbonate dissolution and early diagenesis-implications from an incubation study. *Journal of Marine Research*, 66(4):489–527, 2008.
- [32] W.S. Broecker and T. Takahashi. Calcium carbonate precipitation on Bahama Banks. *Journal of Geophysical Research*, 71(6):1575–&, 1966.
- [33] R.N. Ginsburg and N.P. James. Submarine botryoidal aragonite in Holocene reef limestones, Belize. *Geology*, 4(7):431–436, 1976.

- [34] G.M. Grammer, R.N. Ginsburg, P.K. Swart, D.F. McNeill, A.J.T. Jull, and D.R. Prezbindowski. Rapid growth-rates of syndepositional marine aragonite cements in steep marginal slope deposits, Bahamas and Belize. *Journal of Sedimentary Petrology*, 63(5):983–989, 1993.
- [35] G.M. Grammer, C.M. Crescini, D.F. McNeill, and L.H. Taylor. Quantifying rates of syndepositional marine cementation in deeper platform environments - new insight into a fundamental process. *Journal of Sedimentary Research*, 69(1):202–207, 1999.
- [36] W.S. Broecker, C. Langdon, and T. Takahashi. Factors controlling the rate of CaCO<sub>3</sub> precipitation on Great Bahama Bank. *Global Biogeochemical Cycles*, 15(3):589–596, 2001.
- [37] J.W. Morse, D.K. Gledhill, and F.J. Millero. CaCO<sub>3</sub> precipitation kinetics in waters from the Great Bahama Bank: Implications for the relationship between Bank hydrochemistry and whittings. *Geochimica Et Cosmochimica Acta*, 67(15):2819–2826, 2003.
- [38] R.P. Reid, P.T. Visscher, A.W. Decho, J.F. Stolz, B.M. Bebout, C. Dupraz, L.G. Macintyre, H.W. Paerl, J.L. Pinckney, L. Prufert-Bebout, T.F. Steppe, and D.J. DesMarais. The role of microbes in accretion, lamination and early lithification of modern marine stromatolites. *Nature*, 406(6799):989–992, 2000.
- [39] M.S. Andres, D.Y. Sumner, R.P. Reid, and P.K. Swart. Isotopic fingerprints of microbial respiration in aragonite from Bahamian stromatolites. *Geology*, 34(11):973–976, 2006.
- [40] J.W. Morse, R.S. Arvidson, and A. Luttge. Calcium carbonate formation and dissolution. *Chemical Reviews*, 107(2):342–381, 2007.
- [41] C. Dupraz, R.P. Reid, O. Braissant, A.W. Decho, R.S. Norman, and P.T. Visscher. Processes of carbonate precipitation in modern microbial mats. *Earth-Science Reviews*, 96(3):141–162, 2009.

- [42] T.C.W. Ku, L.M. Walter, M.L. Coleman, R.E. Blake, and A.M. Martini. Coupling between sulfur recycling and syndepositional carbonate dissolution: Evidence from oxygen and sulfur isotope composition of pore water sulfate, South Florida Platform, USA. *Geochimica Et Cosmochimica Acta*, 63(17):2529–2546, 1999.
- [43] D.E. Canfield. Sulfate reduction and oxic respiration in marine-sediments - implications for organic-carbon preservation in euxinic environments. *Deep-Sea Research Part a-Oceanographic Research Papers*, 36(1):121–138, 1989.
- [44] R.E. Zeebe and D.A. Wolf-Gladrow. *CO<sub>2</sub> in seawater: equilibrium, kinetics, isotopes*, volume 65 of *Elsevier Oceanography Series*. Elsevier, Boston, 2001.
- [45] F.J. Millero. The marine inorganic carbon cycle. *Chemical Reviews*, 107(2):308–341, 2007.
- [46] L.A. Anderson. On the hydrogen and oxygen-content of marine-phytoplankton. *Deep-Sea Research Part I-Oceanographic Research Papers*, 42(9):1675–1680, 1995.
- [47] K. Soetaert, A.F. Hofmann, J.J. Middelburg, F.J.R. Meysman, and J. Greenwood. The effect of biogeochemical processes on pH. *Marine Chemistry*, 105(1-2):30–51, 2007.
- [48] J.P. Grotzinger and J.S. Friedman. Occurrence of thick crusts of former botryoidal aragonite, Rifle and Beechey formations (1.97 Ga), Kilohigok Basin, NWT. *Geological Association of Canada Program with Abstract*, 14:A77, 1989.
- [49] C. Summa. *Sedimentologic, stratigraphic, and tectonic controls of a mixed carbonate-siliciclastic succession: Neoproterozoic Johnnie Formation, south-east California*. Ph.D. thesis, 1993.
- [50] S.B. Pruss, F.A. Corsetti, and W.W. Fischer. Seafloor-precipitated carbonate fans in the Neoproterozoic Rainstorm Member, Johnnie Formation, Death Valley Region, USA. *Sedimentary Geology*, 207(1-4):34–40, 2008.

- [51] W.W. Fischer and A.H. Knoll. An iron shuttle for deepwater silica in Late Archean and early Paleoproterozoic iron formation. *Geological Society of America Bulletin*, 121(1-2):222–235, 2009.
- [52] P.A. Sandberg. Aragonite cements and their occurrence in ancient limestone. In N. Schneidermann and P.M. Harris, editors, *Carbonate cements*, volume Special Publication 36, pages 33–57. SEPM, 1985.
- [53] J.P. Grotzinger. Evolution of Early Proterozoic passive-margin carbonate platform, Rocknest Formation, Wopmay Orogen, Northwest-Territories, Canada. *Journal of Sedimentary Petrology*, 56(6):831–847, 1986.
- [54] H.J. Hofmann and G.D. Jackson. Proterozoic ministromatolites with radial-fibrous fabric. *Sedimentology*, 34(6):963–971, 1987.
- [55] J.K. Bartley, A.H. Knoll, J.P. Grotzinger, and V.N. Sergeev. Lithification and fabric genesis in precipitated stromatolites and associated peritidal carbonates, Mesoproterozoic Billyakh Group, Siberia. In J.P. Grotzinger and N.P. James, editors, *Carbonate sedimentation and diagenesis in the evolving Precambrian world*, volume Special Publication 67. SEPM, 2000.
- [56] D.K. Richter, R.D. Neuser, J. Schreuer, H. Gies, and A. Immenhauser. Radial-fibrous calcites: A new look at an old problem. *Sedimentary Geology*, 239:23–36, 2011.
- [57] A.D. Woods, D.J. Bottjer, M. Mutti, and J. Morrison. Lower Triassic large sea-floor carbonate cements: Their origin and a mechanism for the prolonged biotic recovery from the end-Permian mass extinction. *Geology*, 27(7):645–648, 1999.
- [58] A.D. Woods, D.J. Bottjer, and F.A. Corsetti. Calcium carbonate seafloor precipitates from the outer shelf to slope facies of the Lower Triassic (Smithian-Spathian) Union Wash Formation, California, USA: Sedimentology and palaeobiologic significance. *Palaeogeography Palaeoclimatology Palaeoecology*, 252(1-2):281–290, 2007.

- [59] A.D. Woods and A. Baud. Anachronistic facies from a drowned Lower Triassic carbonate platform: Lower member of the Alwa Formation (Ba'id Exotic), Oman Mountains. *Sedimentary Geology*, 209(1-4):1–14, 2008.
- [60] J.P. Grotzinger and D.S. McCormick. Flexure of the Early Proterozoic lithosphere and the evolution of Kilohigok Basin (1.9 Ga), Northwest Canadian Shield. pages 405–430. Springer-Verlag, New York, 1988.
- [61] C. Klein and R.P. Fink. Petrology of Sokoman Iron Formation in Howells River area, at western edge of Labrador Trough. *Economic Geology*, 71(2):453–487, 1976.
- [62] B.M. Simonson. Sedimentological constraints on the origins of Precambrian iron-formations. *Geological Society of America Bulletin*, 96(2):244–252, 1985.
- [63] B.M. Simonson. Early silica cementation and subsequent diagenesis in arenites from 4 early Proterozoic iron formations of North America. *Journal of Sedimentary Petrology*, 57(3):494–511, 1987.
- [64] N.J. Beukes and C. Klein. Geochemistry and sedimentology of a facies transition - from microbanded to granular iron-formation - in the Early Proterozoic Transvaal Supergroup, South Africa. *Precambrian Research*, 47(1-2):99–139, 1990.
- [65] W.W. Fischer, S. Schroeder, J.P. Lacassie, N.J. Beukes, T. Goldberg, H. Strauss, U.E. Horstmann, D.P. Schrag, and A.H. Knoll. Isotopic constraints on the Late Archean carbon cycle from the Transvaal Supergroup along the western margin of the Kaapvaal Craton, South Africa. *Precambrian Research*, 169(1-4):15–27, 2009.
- [66] R.M. Hotinski, L.R. Kump, and M.A. Arthur. The effectiveness of the Paleoproterozoic biological pump: A delta C-13 gradient from platform carbonates of the Pethei Group (Great Slave Lake Supergroup, NWT). *Geological Society of America Bulletin*, 116(5-6):539–554, 2004.

- [67] F.A. Corsetti and A.J. Kaufman. Stratigraphic investigations of carbon isotope anomalies and Neoproterozoic ice ages in Death Valley, California. *Geological Society of America Bulletin*, 115(8):916–932, 2003.
- [68] F.A. Corsetti, A. Baud, P.J. Marenco, and S. Richoz. Summary of early Triassic carbon isotope records. *Comptes Rendus Palevol*, 4(6-7):473–486, 2005.
- [69] R. Petterson, A.R. Prave, B.P. Wernicke, and A.E. Fallick. The Neoproterozoic Noonday Formation, Death Valley region, California. *Geological Society of America Bulletin*, 123(7-8):1317–1336, 2011.
- [70] A.J. Kaufman, F.A. Corsetti, and M.A. Varni. The effect of rising atmospheric oxygen on carbon and sulfur isotope anomalies in the Neoproterozoic Johnnie Formation, Death Valley, USA. *Chemical Geology*, 237(1-2):47–63, 2007.
- [71] K.D. Bergmann, R.A. Zentmyer, and W.W. Fischer. The stratigraphic expression of a large negative carbon isotope excursion from the Ediacaran Johnnie Formation, Death Valley. *Precambrian Research*, 188:45–56, 2011.
- [72] J.P. Grotzinger, D.A. Fike, and W.W. Fischer. Enigmatic origin of the largest-known carbon isotope excursion in Earth’s history. *Nature Geoscience*, 4(5):285–292, 2011.
- [73] C. Verdel, B.P. Wernicke, and S.A. Bowring. The Shuram and subsequent Ediacaran carbon isotope excursions from southwest Laurentia, and implications for environmental stability during the metazoan radiation. *Geological Society of America Bulletin*, 123(7/8):1539–1559, 2011.
- [74] M.A. Wilson and T.J. Palmer. *Hardgrounds and Hardground Faunas*. Issue 9 of University of Wales, Aberystwyth, Institute of Earth Science Publications. University of Wales, Aberystwyth, 1992.
- [75] R.M. Burkhalter. Ooidal ironstones and ferruginous microbialites - origin and relation to sequence stratigraphy (Aalenian and Bajocian, Swiss Jura Mountains). *Sedimentology*, 42(1):57–74, 1995.

- [76] B.M. Simonson and S.W. Hassler. Was the deposition of large Precambrian iron formations linked to major marine transgressions? *Journal of Geology*, 104(6):665–676, 1996.
- [77] P. Fralick and P.K. Pufahl. Iron formation in Neoproterozoic deltaic successions and the microbially mediated deposition of transgressive systems tracts. *Journal of Sedimentary Research*, 76(9-10):1057–1066, 2006.
- [78] J.C.G. Walker. Suboxic diagenesis in banded iron formations. *Nature*, 309(5966):340–342, 1984.
- [79] S.W. Poulton, D.E. Canfield, and P. Fralick. Development of a global sulfidic ocean at similar to 1.84 Ga: Evidence from Fe-S systematics in the Rove Formation, Ontario. *Geochimica Et Cosmochimica Acta*, 68(11):A797–A797, 2004.
- [80] P. Kharecha, J. Kasting, and J. Siefert. A coupled atmosphere-ecosystem model of the early Archean Earth. *Geobiology*, 3(2):53–76, 2005.
- [81] D.Y. Sumner and J.P. Grotzinger. Implications for Neoproterozoic ocean chemistry from primary carbonate mineralogy of the Campbellrand-Malmani Platform, South Africa. *Sedimentology*, 51(6):1273–1299, 2004.
- [82] J.K. Bartley and L.C. Kah. Marine carbon reservoir, C-org-C-carb coupling, and the evolution of the Proterozoic carbon cycle. *Geology*, 32(2):129–132, 2004.
- [83] T.M. Peryt, A. Hoppe, T. Bechstadt, J. Koster, C. Pierre, and D.K. Richter. Late Proterozoic aragonitic cement crusts, Bambui Group, Minas-Gerais, Brazil. *Sedimentology*, 37(2):279–286, 1990.
- [84] D.E. Canfield and J. Farquhar. Animal evolution, bioturbation, and the sulfate concentration of the oceans. *Proceedings of the National Academy of Sciences of the United States of America*, 106(20):8123–8127, 2009.

- [85] M.L. Droser and D.J. Bottjer. Trends and patterns of Phanerozoic ichnofabrics. *Annual Review of Earth and Planetary Sciences*, 21:205–225, 1993.
- [86] S.M. Kidwell and P.J. Brenchley. Patterns in bioclastic accumulation through the phanerozoic - changes in input or in destruction. *Geology*, 22(12):1139–1143, 1994.
- [87] R.K. Bambach. Phanerozoic biodiversity mass extinctions. *Annual Review of Earth and Planetary Sciences*, 34:127–155, 2006.
- [88] J.J. Sepkoski. A model of onshore-offshore change in faunal diversity. *Paleobiology*, 17(1):58–77, 1991.
- [89] S.J. Mazzullo and J.M. Cys. Marine aragonite sea-floor growths and cements in Permian phylloid algal mounds, Sacramento Mountains, New Mexico. *Journal of Sedimentary Petrology*, 49(3):917–936, 1979.
- [90] Y. Isozaki. Permo-Triassic Boundary superanoxia and stratified superocean: Records from lost deep sea. *Science*, 276:235–238, 1997.
- [91] C.Q. Cao, G.D. Love, L.E. Hays, W. Wang, S.Z. Shen, and R.E. Summons. Biogeochemical evidence for euxinic oceans and ecological disturbance presaging the end-Permian mass extinction event. *Earth and Planetary Science Letters*, 281(3-4):188–201, 2009.
- [92] G.A. Logan, J.M. Hayes, G.B. Hieshima, and R.E. Summons. Terminal Proterozoic reorganization of biogeochemical cycles. *Nature*, 376(6535):53–56, 1995.
- [93] P.B. Wignall. *Black Shales*. Oxford Monographs Geol. Geophys. Oxford University Press, Oxford, 1994.